JGP Journal of General Physiology

ARTICLE

The C-terminus of Rad is required for membrane localization and L-type calcium channel regulation

Garrett Elmore[1*], Brooke M. Ahern[1*], Nicholas M. McVay[1], Kyle W. Barker[1], Sarisha S. Lohano[1], Nemat Ali[2], Andrea Sebastian[1], Douglas A. Andres[2], Jonathan Satin[1], and Bryana M. Levitan[1,3]

L-type $Ca_V1.2$ current ($I_{Ca,L}$) links electrical excitation to contraction in cardiac myocytes. $I_{Ca,L}$ is tightly regulated to control cardiac output. Rad is a Ras-related, monomeric protein that binds to L-type calcium channel β subunits ($Ca_V\beta$) to promote inhibition of $I_{Ca,L}$. In addition to $Ca_V\beta$ interaction conferred by the Rad core motif, the highly conserved Rad C-terminus can direct membrane association in vitro and inhibition of $I_{Ca,L}$ in immortalized cell lines. In this work, we test the hypothesis that in cardiomyocytes the polybasic C-terminus of Rad confers t-tubular localization, and that membrane targeting is required for Rad-dependent $I_{Ca,L}$ regulation. We introduced a 3xFlag epitope to the N-terminus of the endogenous mouse *Rrad* gene to facilitate analysis of subcellular localization. Full-length 3xFlag-Rad (Flag-Rad) mice were compared with a second transgenic mouse model, in which the extended polybasic C-termini of 3xFlag-Rad was truncated at alanine 277 (Flag-RadΔCT). Ventricular cardiomyocytes were isolated for anti-Flag-Rad immunocytochemistry and ex vivo electrophysiology. Full-length Flag-Rad showed a repeating t-tubular pattern whereas Flag-RadΔCT failed to display membrane association. $I_{Ca,L}$ in Flag-RadΔCT cardiomyocytes showed a hyperpolarized activation midpoint and an increase in maximal conductance. Additionally, current decay was faster in Flag-RadΔCT cells. Myocardial $I_{Ca,L}$ in a Rad C-terminal deletion model phenocopies $I_{Ca,L}$ modulated in response to β-AR stimulation. Mechanistically, the polybasic Rad C-terminus confers $Ca_V1.2$ regulation via membrane association. Interfering with Rad membrane association constitutes a specific target for boosting heart function as a treatment for heart failure with reduced ejection fraction.

Introduction

L-type $Ca_V1.2$ current ($I_{Ca,L}$) links electrical excitation to contraction in cardiac myocytes. $I_{Ca,L}$ is tightly regulated to control cardiac output. During stress or exercise when higher cardiac output is demanded, sympathetic input via the β-adrenergic receptor/adenyl cyclase/cAMP/protein kinase A (PKA) cascade results in positive inotropy and lusitropy in contractile cardiomyocytes (Bers, 2002). PKA modulates $I_{Ca,L}$ where modulation of $Ca_V1.2$ is defined as increased $I_{Ca,L}$ amplitude, shifted activation midpoint to a more negative potential, and faster current decay (Bers, 2008).

The L-type Ca^{2+} channel is a heteromultimeric protein complex. Members of the RGK (Rad, Rem, Rem2, and Gem/Kir) subfamily of small Ras-related G-proteins bind to auxiliary $Ca_V\beta$ subunits and govern L-type calcium channel function (Béguin et al., 2001; Finlin et al., 2003). Ras associated with diabetes (Rad, gene name *Rrad*) was first identified in the skeletal and cardiac muscle of humans with type II diabetes mellitus (Reynet and Kahn, 1993). In heterologous expression systems, a shared property among all RGK proteins is interaction with $Ca_V\beta$-subunits and inhibition of $I_{Ca,L}$ (Béguin et al., 2001, 2005; Finlin et al., 2003; Murata et al., 2004; Ward et al., 2004; Chen et al., 2005) via several potential mechanisms including voltage sensor immobilization (Yang et al., 2010), reduced channel open probability, and reduced cell surface expression of Ca_V1 channels (Finlin et al., 2003; Béguin et al., 2006; Correll et al., 2008b; Pang et al., 2010; Sasson et al., 2022, *Preprint*). Rad has been shown to use both $Ca_V\beta$-binding-dependent and -independent mechanisms for channel regulation (Yang et al., 2012). Early heterologous expression studies showed that the polybasic C-terminus of Rem is required for membrane targeting and $I_{Ca,L}$ regulation (Correll et al., 2007; Pang et al., 2010). The RGK C-terminus is highly conserved among family members, suggesting parallel mechanisms for Rad regulation of $I_{Ca,L}$ in cardiomyocytes.

[1]Department of Physiology, University of Kentucky, Lexington, KY, USA; [2]Department of Molecular and Cellular Biochemistry, University of Kentucky, Lexington, KY, USA; [3]Gill Heart and Vascular Institute, Lexington, KY, USA.

Correspondence to Jonathan Satin: jsatin1@uky.edu

*G. Elmore and B.M. Ahern shared co-first authors.

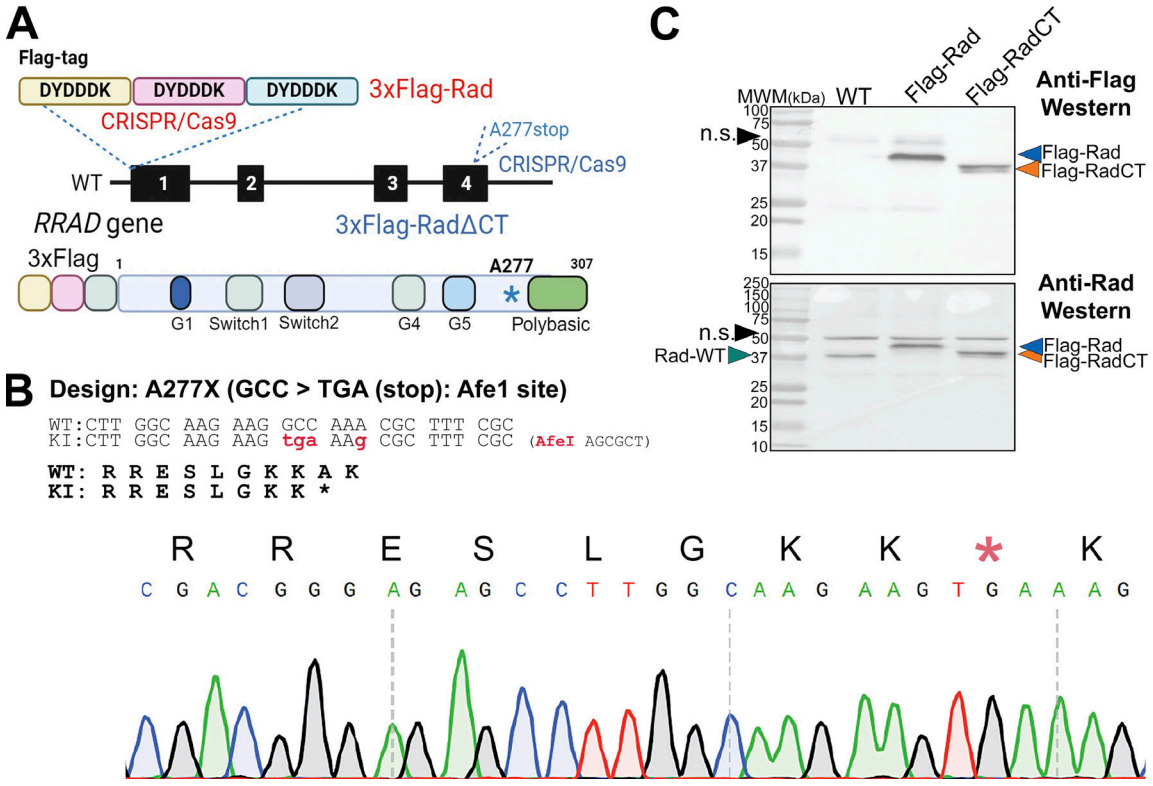

Figure 1. **Generation of Flag-Rad knock-in mice. (A)** Graphical representation of the *RRAD* gene engineering strategy. Two transgenic mouse models were generated with CRISPR/Cas9 targeting the endogenous *RRAD* gene in this study. First, a 3xFlag epitope was inserted at the N-terminus of *RRAD*, generating 3xFlag-Rad mice. Subsequent CRISPR/Cas9 engineering of 3xFlag-Rad embryo introduced a stop codon at amino acid position 277, removing a large portion of the polybasic C-terminus of Rad important for membrane anchoring in cultured cells (Flag-RadΔCT). Created with BioRender.com. **(B)** Validation of stop codon knock-in showing the location of base changes (upper) and stop codon insertion in place of Ala277 (lower). **(C)** Western blot for Rad and Flag-Rad expression in protein lysates from wildtype (WT), Flag-Rad, and Flag-RadΔCT whole heart lysates. Note that total Rad protein levels are not significantly changed in either transgenic model. Source data are available for this figure: SourceData F1.

Heterologous expression studies have proven invaluable for understanding RGK-regulation of $I_{Ca,L}$, but data interpretation is limited because of the impossibility of recapitulating native stoichiometries of the multitude of proteins with overlapping interaction domains located within the cardiac L-type Ca^{2+}-channel complex (Satin, 2017). We recently demonstrated that myocardial-restricted Rad knockout results in a sustained increase of inotropy without structural or functional remodeling of the heart (Ahern et al., 2019), consistent with a role for Rad as an endogenous negative regulator of $Ca_V1.2$ voltage-gated calcium channels (Ahern et al., 2019). Using proximity proteomics, Liu et al. (2020) reported that Rad is adjacent to the $Ca_V1.2$ channel complex in mouse hearts, but is depleted in response to acute β-adrenergic stimulation, suggesting that PKA phosphorylation leads to dissociation of Rad from the $Ca_V1.2$ complex. The purpose of this study was to address unanswered questions: (1) what is the native subcellular distribution of Rad in cardiomyocytes, and is this distribution altered in response to adrenergic signaling; and, (2) what role does the C-terminus play in control of Rad function. To address these issues, we created two Rad transgenic mouse models: the first was engineered with an N-terminal Flag affinity tag to permit facile immunohistological detection of endogenous Rad protein in cardiomyocytes. The second transgenic mouse model expresses endogenous levels of Flag-tagged Rad bearing a truncation of Rad in the C-terminus to allow analysis of the contribution of this domain to subcellular localization and channel regulation. Using these engineered mouse models, we find that Rad is localized in a striated pattern in cardiomyocytes, in a manner that requires the conserved polybasic C-terminus. Moreover, loss of membrane localization results in a phenotype which mirrors that arising from complete Rad knockout.

Materials and methods

Animal model

All experimental procedures and protocols were approved by the Animal Care and Use Committee of the University of Kentucky Cincinnati Children's Hospital and conformed to the National Institute of Health's "Guide for the Care and Use of Laboratory Animals."

Flag-Rad knock-in mice

Genome editing was performed by the staff at the Transgenic Animal and Genome Editing Core (TAGE) at Cincinnati Children's Hospital. CRISPR/Cas9 gene engineering was used to introduce first a 3xFlag epitope tag to the N-terminus of the endogenous mouse *Rrad* gene, with offspring screened by

genomic PCR analysis, and insertion of the 3xFlag epitope confirmed by Sanger sequencing, resulting in a mouse expressing 3xFlag-Rad under control of its native promoter (Flag-Rad). A second round of CRISPR/Cas9 genome-editing was used to modify the 3xFlag-tagged Rad mouse, introducing a stop codon at Ala277 within the extended C-terminus of the *RRad* gene to generate a second transgenic mouse expressing 3xFlag-Rad bearing a C-terminal truncation (see Fig. 1 A; herein abbreviated Flag-RadΔCT). The sgRNA's for the A277stop insertion were engineered to contain an AfeI site, with offspring screened by genomic PCR analysis/AfeI digestion, and the inclusion of both the 3xFlag tag and A277 stop codon confirmed by Sanger sequencing (Fig. 1 B). The authenticity of the models was further supported by Western blot analysis of heart lysates from Flag-Rad and Flag-RadΔCT mice (Fig. 1 C). For a Flag-negative control, cardiomyocytes were dispersed from the hearts of cardiomyocyte-restricted Rad-knockout mice as previously described (Ahern et al. 2019).

Ventricular myocyte isolation

Ventricular cardiomyocytes were prepared as previously described (Magyar et al., 2012). Prior to heart excision, mice were euthanized by first anesthesia with ketamine + xylazine (90 + 10 mg/kg intraperitoneal) followed by cervical luxation. Hearts were excised from adult mice (3–7 mo of age) and immediately perfused on a Langendorff apparatus with a high-potassium Tyrode buffer and then digested with 5–7 mg liberase (05401135001; Sigma-Aldrich). After digestion, atria were removed and ventricular myocytes were mechanically dispersed. Calcium concentrations were gradually restored to physiological levels in a stepwise fashion, and the criteria for inclusion/exclusion was that only healthy quiescent ventricular myocytes were used for electrophysiological analysis within 8 h. Researchers were blinded to genotype for data collection and analysis. For β-adrenergic receptor agonist studies using immunocytochemistry studies, drug treatment was randomized across aliquots of cells from each dispersal. In lieu of power analysis, sample sizes were determined a priori based on published literature for electrophysiological recordings and adult cardiomyocyte immunocytochemistry. Female mice were used for cellular experiments. In experiments using these isolated cells, mice were considered as biological replicates. In the main and supplemental figures, every mouse and cell as individual data points are shown, and nested statistics were used to treat mice as biological replicates (see Statistics). For anti-Flag microscopy, two to four technical replicate images of different regions of each cell were collected and averaged into one cell average. Detailed sample sizes for each experiment and replicates are reported in figure legends.

Electrophysiological recordings

$I_{Ca,L}$ was recorded in the whole-cell configuration of the patch-clamp technique as previously described (Magyar et al., 2012). All recordings were performed at room temperature (20°–22°C). Borosilicate glass pipettes fire-polished to a resistance of 800–3,000 kΩ were filled with a solution consisting of (in mmol/liter) 125 Cs-methano-sulfonate, 15 TEA-Cl, 1 $MgCl_2$, 10 EGTA, 5 HEPES, 5 Mg-ATP, and 5 phosphocreatine, pH 7.2. Physiological Tyrodes bath solution contained (in mmol/liter) 140 NaCl, 5.4 KCl, 1.2 KH_2PO_4, 5 HEPES, 5.55 glucose, 1 $MgCl_2$, and 1.8 $CaCl_2$, pH 7.4. After whole-cell access was achieved, zero sodium bath solution was introduced into the chamber consisting of (in mmol/liter) 150 NMDG, 2.5 $CaCl_2$, 1 $MgCl_2$, 10 glucose, 10 HEPES, 0.0313 tetrodotoxin citrate, and 5 4-AP, pH 7.2. L-type calcium currents were evoked by 300-ms depolarizing voltage steps starting from V_{rest} of −80 mV in +5 mV increments up to +40 mV at 5 s intervals. β-Adrenergic receptor agonist response was recorded in zero sodium bath solution containing 300 nM isoproterenol (ISO) using a 200-ms voltage ramp from −80 to +60 mV repeated once every 3 s. Currents were sampled at 10 kHz. A low-pass filter was applied using an Axopatch 200B (Molecular Devices), digitized with an Axon Digidata 1550B (Molecular Devices), acquired with Clampex 11.2 (Molecular Devices). Clampfit 11.2 (Molecular Device) was used for analysis. Activation voltage dependence parameters were obtained by fitting the current–voltage slope conductance transform to a Boltzmann distribution of the form $G(V) = G_{max}/[1 + \exp(V½/k)]$, where G_{max} is the maximal conductance and V½ is the activation midpoint. GraphPad Prism 10.1 was used to fit the current–voltage slope conductance transform to a Boltzmann distribution of the form $G(V) = G_{max}/[1 + \exp(V½/k)]$, where G_{max} is the maximal conductance and V½ is the activation midpoint to determine activation voltage dependence parameters. For current decay kinetics, expressed as r30 and r150, traces were normalized to peak $I_{Ca,L}$, and then mean amplitude was measured at 30 and 150 ms after the peak. The remaining current was then calculated by subtracting the mean amplitude from 1.

Echocardiography

Transthoracic echocardiography was performed using the Vevo 3100 high-resolution imaging system equipped with a MX550D (25–55 MHz) linear transducer (FujiFilm, VisualSonics, Inc.). Mice were first anesthetized with 2% isoflurane in an induction chamber, chest hair was removed prior to imaging, then a nose cone was placed with inhaled isoflurane, (0.5–1% + 0.5–1.0 liter/min 100% O_2) to maintain a light anesthesia level, with heart rate (350–500 beats per minute) and core temperature (37°C) continuously monitored and maintained by a heated platform. Male and female mice were evaluated. The heart was visualized from the modified parasternal long-axis and short-axis views. The left ventricular dimensions and calculated left ventricular EF were measured from the short-axis M-mode view (Zacchigna et al., 2021). For ISO echocardiography stress testing, mice were injected intraperitoneally with ISO (10 mg/kg) after the baseline long- and short-axis M-mode images and B-mode cine loops of the left ventricle were acquired. The peak stress short-axis M-mode images and B-mode cine loops of the left ventricle were acquired 1–3 min after ISO was given, allowing for a maximal stable increase in heart rate and contractility. Each mouse consisted of three technical replicates that were averaged. Power analysis was not used prior to the study. The sonographer was blinded to animal genotype, and data analysis was performed with animal genotype blinded.

Immunoblotting

Freshly excised hearts were flash-frozen, and the tissue was pulverized before sonication in cell lysis buffer containing (in

mmol/liter) 50 Hepes, pH 7.5, 150 NaCl, 0.5% Triton X 100, 1 EDTA, 1 EGTA, 10 NaF, 2.5 NaVO4, complete Protease Inhibitor Cocktail (11697498001; Sigma-Aldrich), Phosphatase Inhibitor Cocktail 2 (P5726; Sigma-Aldrich), and Phosphatase Inhibitor Cocktail 3 (P0044; Sigma-Aldrich). Lysates were centrifuged at 14,000 rpm and protein concentrations of supernatants were measured. Lysates were analyzed on 4–20% (anti-$Ca_V1.2$) or 15% SDS PAGE gels. Immunoblotting was performed with anti-Rad (1:2,000, EB11418; Everest Biotech), anti-Flag (1:500, F1804, RRID:AB_262044; Sigma-Aldrich), and anti-$Ca_V1.2$ (1:500, ACC-003, RRID:AB_2039771; Alomone) antibodies. Proteins were detected using SuperSignal enhanced chemiluminescence (Pierce) or luminol/enhancer solution: peroxide solution (anti-$Ca_V1.2$) (Bio-Rad). Immunoblots were developed and quantified using the Bio-Rad ChemiDoc MP Imaging System. Total protein loading was assessed by staining the membranes with Ponceau S staining (data not shown). $Ca_V1.2$ protein quantification was determined with Bio-Rad Image lab software and quantified relative to total protein for each lane (stain free total protein measurement).

Microscopy

No. 1.5H coverslips were coated with poly-*L* lysine before plating freshly dispersed ventricular murine cardiomyocytes that were allowed to adhere in an incubator (37°C) for 30 min. Cells were then fixed with 4% paraformaldehyde in phosphate-buffered saline (PBS) for 10 min; a subset of coverslips were treated with ISO, (1 µM) for 3 min before fixing. Cells were washed thrice before permeabilization with 0.5% triton-X100 in PBS for 10 min. Cells were washed again before blocking for at least 1 h with 3% bovine serum albumin with 0.5% triton in PBS. After washing, cells were incubated with primary antibody in 3% bovine serum albumin in PBS overnight at 4°C. Primary antibodies used were Sigma-Aldrich F1804 mouse IgG1 anti-Flag at 1 µg/ml, Alomone Labs ACC-003 Rabbit IgG anti-$Ca_V1.2$ at 2.67 µg/ml, and Invitrogen (701914) α-actinin 2 Rabbit IgG (clone: 7H1L69) at 1 µg/ml. The next day, after washing, cells were incubated for 1 h with secondary antibodies: Invitrogen A21202 Alexa Fluor 488 donkey anti-mouse IgG (H+L) at 2 µg/ml and Invitrogen Alexa Fluor A11011 568 goat anti-rabbit IgG (H+L) at 4 µg/ml. After washing, Invitrogen ProLong Glass Antifade Mountant (P36982) 1.52 refractive index hard setting mounting media was used to mount coverslips onto glass slides. The mounting media was allowed to cure for at least 60 h before imaging. A Nikon A1R confocal microscope (Nikon) and Nikon Super Resolution Microscope equipped with a Structured Illumination Microscopy (SIM) module (Nikon) with an oil-immersion CFI Apo 100×/1.49 NA TIRF objective (v) was used. Excitation wavelengths 488 and 561 nm were used to excite Alexa Fluor 488 and Alexa Fluor 568 secondary antibodies, respectively. To quantify the regularity in the periodic signal of Flag, fluorescence intensity plot profiles of confocal micrographs were analyzed via fast Fourier transform (FFT), following methodology performed by other groups analyzing t-tubule and t-tubular protein expression in cardiomyocytes (Hong et al., 2010; Guo and Song, 2014). Intensity plot profiles of rectangular regions of interest of the same size free of nuclear signal were collected from raw 16-bit confocal images using ImageJ (Schneider et al., 2012). A FFT analysis was written in MATLAB (MathWorks) and applied to the exported regions of interest. Individual images of a cell were considered technical replicates and averaged to produce the peak FFT power for a given cell. For live cell t-tubular staining, unladdered isolated ventricular cardiomyocytes were loaded with 10 µM Di-8-ANEPPS (sc-214873; Santa Cruz) for 10 min then washed thrice. Cells were imaged on glass (#1.5) bottom dishes at room temperature with a Nikon AX-R confocal microscope (Nikon) with a Nikon oil-immersion Plan Apo 60×/1.42 NA using an excitation wavelength of 488 nm. T-tubular periodicity was quantified with FFT analysis of fluorescence intensity profiles using MATLAB (RRID: SCR_001622) as done with the anti-Flag FFT analysis. Resting sarcomere length of live cells was measured with brightfield microscopy utilizing a Nikon Eclipse TE200 (Nikon), a Nikon oil-immersion plan fluor 40×/1.30 NA objective, IonOptix MyoCam-S3, MyoPacer Field Stimulator, and Fluorescence System Interface, and analyzed via IonWixard v7.5.3.165. Cells at room temperature were paced at 1 Hz to induce a steady state. Researchers were blinded to genotype when scoring confocal micrographs for t-tubular patterns of anti-Flag staining, and a minimum of five regularly spaced vertical signals was the criteria in consideration of an observed t-tubular-like expression. Mice and cell sample sizes are in figure legends. Only images in which both blinded researchers independently from each other identified expression were counted as true expression.

Computational modeling of Rad and C-terminus truncated Rad with the plasma membrane

AlphaFold (AlphaFold2_mmseqs2 notebook of ColabFold; Deepmind) (Jumper et al., 2021; Mirdita et al., 2022) was used to generate a PDB file of a C-termini truncation of the polybasic α-helix that corresponds to replacing amino acid 277 alanine with a stop codon of murine Rad. The generated PDB file was then processed using PPM 3.0 web tool to visualize the orientations of proteins in membranes (Lomize et al., 2012, 2022) and to determine predicted residue interactions with a mammalian plasma membrane. The tool was also used for the AlphaFold full-length *Mus musculus* Rad PDB file. As per PPM 3.0 authors' recommendation, AlphaFold regions with very low confidence (pLDDT < 50) were removed before modeling with PPM 3.0 (residues 1–89; 296–308 were excluded). The graphics of the PDB files outputted from PPM 3.0 were generated using the National Center for Biotechnology Information tool, iCn3D (Wang et al., 2020, 2022).

Statistical analysis

In figures, data are presented as the mean ± SEM unless represented by a box and whisker plot in which case the medians (line), mean (+), and min to max (whiskers) are reported. Linear mixed models were used in experiments that had a hierarchical/nested structure of cells being sampled from the same mouse and treated mice as a random factor with genotype as a fixed factor. Normality and equality of variances were assessed visually and via normality (Shapiro-Wilk) and variance (Levene's) tests. The P values of pairwise comparisons were corrected for multiple comparisons using Holm adjustment of estimated

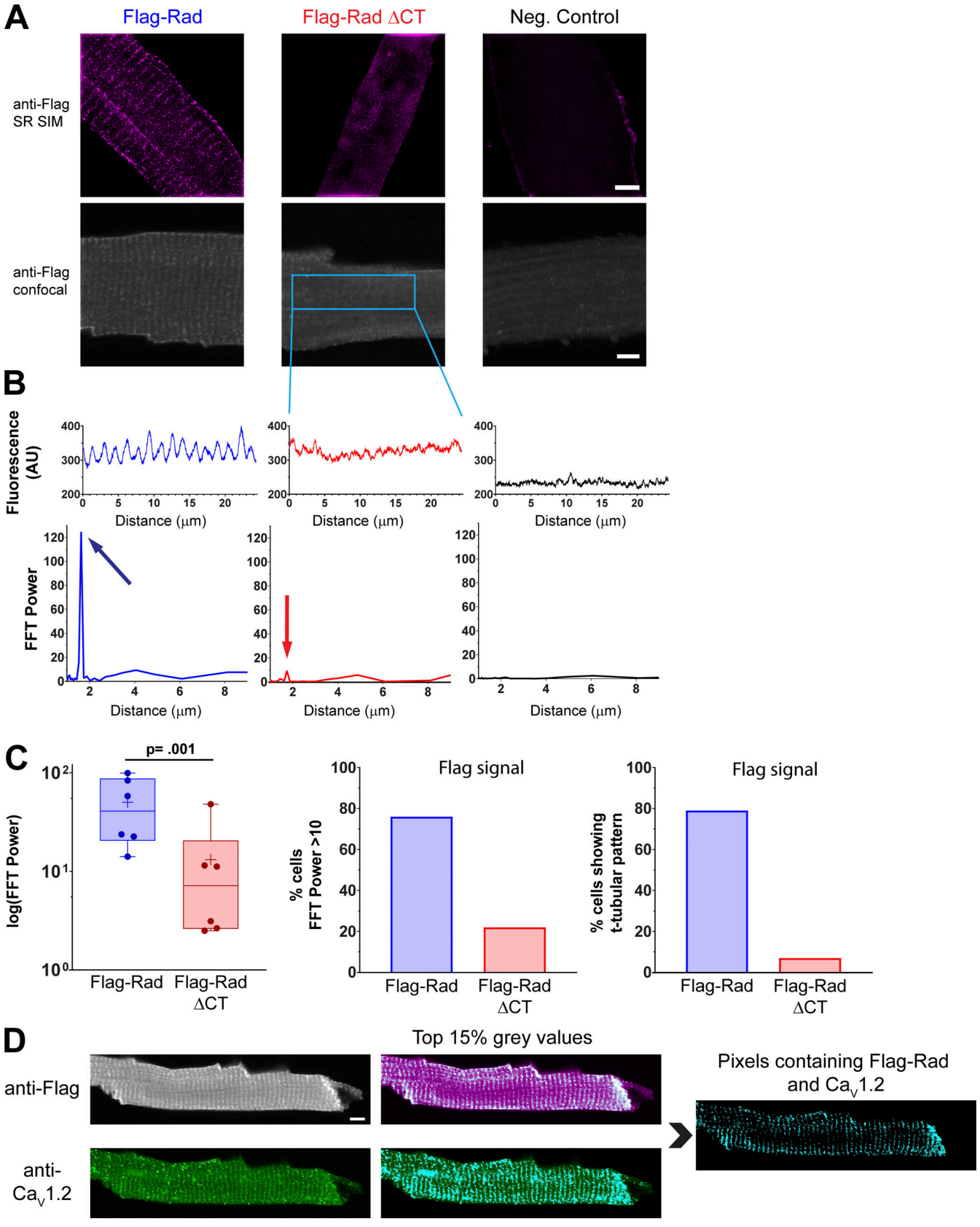

Figure 2. **The C-terminus tail of Rad is necessary for t-tubular expression in adult murine ventricular cardiomyocytes. (A)** SR SIM maximum intensity projections of fixed adult murine cardiomyocytes stained with anti-Flag to visualize Flag tagged Rad in two transgenic mice, full-length Flag-Rad, and C-terminus ablated Flag-RadΔCT. A no primary antibody control image is provided using the same acquisition and brightness and contrast settings. Scale bar,

5 µm; magnification is the same for all images. **(B)** Confocal micrographs of adult murine cardiomyocytes from Flag-Rad or Flag-RadΔCT. As a negative control for Flag immunofluorescence, a cardiomyocyte from a Rad knockout mouse is shown (right panel). Scale bar, 5 µm. Fluorescence intensity profiles of regions of interest from the representative images and their FFT power spectrums. **(C)** Fundamental peak power of anti-Flag immunostaining that represents a signal with periodicity consistent with t-tubular expression. The FFT peak power median of Flag-Rad 40.9 (IQR: 20.4-87.6; *N* = 6 mice, *n* = 41 cells, 93 images) was significantly 476% higher than Flag-RadΔCT 7.1 (IQR: 2.6-20.6; *N* = 6 mice, *n* = 41 cells, 92 images). Statistical significance was determined by a linear mixed model, nesting cells into the random factor mouse. Genotype as a main effect was significantly different (P = 0.002, F = 16.502). The estimated marginal means contrast with P value adjustment (Holm) for multiple comparisons (see Fig. 5) between the Flag-Rad and Flag-RadΔCT cells untreated was significantly different (P = 0.001). Boxes are interquartile ranges and whiskers, min to max. 76% of Flag-Rad versus 22% of Flag-RadΔCT cells had FFT power >10. Blinded researchers identified 79% of Flag cells and 7% of Flag-RadΔCT cells as having Flag-staining in an organized t-tubular pattern in at least one region of the cell. Two to four technical replicate images' FFT power was averaged per cell. **(D)** A Flag-Rad cardiomyocyte was stained for anti-Flag Rad and anti-$Ca_V1.2$. The top 15% gray value intensities are highlighted in cyan in both micrographs. The last micrograph shows pixels that contain both anti-Flag and anti-$Ca_V1.2$ staining if that pixel was in the top 15% of gray values in both channels. Scale bar, 5 µm; magnification is the same for all images.

marginal means. The means and their 95% confidence intervals are reported in the figure legends. In experiments that did not have nested structure, parametric two-sample t-tests or non-parametric Mann–Whitney *U* test was used for comparisons of two groups, unpaired. For the repeated-measures echocardiography ISO stress test, a three-way ANOVA considering basal (before) versus (after) ISO, sex, and genotype was performed. Since sex as a main effect was not significantly different, separate two-way repeated measures ANOVA's were used for males and females to focus on the primary questions of genotype and ISO treatment effects. Sidak's multiple comparison test was used post-hoc to correct for multiple comparisons. For the microscopy FFT data that contained cells fixed with or without drug exposure thus having fixed factors of genotype and drug treatment, the data was right-skewed, not normally distributed, and had unequal variances, and thus was log10 transformed for statistical analysis to mitigate violations of linear mixed model assumptions. For all statistical tests, α was 0.05. Statistical analysis was performed using GraphPad Prism 10.1 (RRID:SCR_002798) and JASP 0.18.3. (JASP Team, 2024) RRID:SCR_015823.

Results

Generation of Flag-Rad and Flag-RadΔCT transgenic mice

Studies in heterologous expression systems showed that the polybasic C-terminal domain of Rad is necessary for membrane anchoring and regulation of the L-type Ca^{2+} channel; however, non-native systems cannot recapitulate cardiomyocyte L-type Ca^{2+} channel constituents and stoichiometries. To permit analysis of the subcellular distribution of endogenous Rad protein, CRISPR/Cas9 technologies were used to genetically target *RRad*, introducing three copies of the Flag epitope to the N-terminus of the *RRad* gene (3xFlag-Rad, see Fig. 1 A). To examine the importance of the conserved C-terminus to Rad function, a second round of CRISPR/Cas9 engineering was used to introduce a stop codon at amino acid position Ala277 using embryos from the 3xFlag-Rad mouse, generating the 3xFlag-RadΔCT mouse model lacking the conserved C-terminal domain (Fig. 1 A). Successful generation of the mouse models was confirmed by Sanger sequencing and Western blot analysis performed on heart ventricle tissue lysates (Fig. 1 B). Importantly, both Flag-Rad and Flag-RadΔCT were expressed at levels indistinguishable from that of endogenous Rad protein. As expected, the Flag-Rad protein migrated more slowly than native Rad on SDS-PAGE, and the 31-amino acid C-terminal deletion in Flag-RadΔCT resulted in a protein that migrated closer to that of endogenous Rad (Fig. 1 C).

The C-terminus of Rad is necessary for membrane localization in cardiomyocytes

Rad is known to bind to $Ca_V\beta$ and regulate $I_{Ca,L}$, but to date, there have been no investigations of Rad localization in cardiomyocytes. Furthermore, if the C-terminus tail of Rad plays a role in membrane localization allowing for interaction with $Ca_V1.2$ in t-tubules, we hypothesize that truncated Rad (Flag-RadΔCT) will display significantly reduced t-tubular localization. Super-resolution structured illumination microscopy (SR SIM) micrographs of primary cardiomyocytes isolated from Flag-Rad mice exhibit regularly spaced signals consistent with t-tubular periodicity (Fig. 2 A and Video 1) as reported in the literature of stained t-tubules or junctional dyad proteins such as $Ca_V1.2$ (Soeller and Cannell, 1999; Hong et al., 2010; Maleckar et al., 2017; Ito et al., 2019). By contrast, Flag-RadΔCT cells presented with diffuse immunofluorescent staining (Fig. 2 A and Video 2). To quantify the regularity in the periodic signal of Flag-Rad staining (Fig. S2 A), fluorescence intensity plot profiles of confocal micrographs were analyzed via FFT, following a methodology applied by other groups for analyzing t-tubule and t-tubular protein expression in cardiomyocytes (Hong et al., 2010; Guo and Song, 2014) (Fig. 2 B). Median Flag-Rad FFT power was significantly higher (476%) than Flag-RadΔCT (Fig. 2 C). 79% of Flag-Rad cells were classified by blinded researchers as having organized t-tubular expression in at least one region of the cell, an observation corroborated by 76% of Flag-Rad cells showing well-powered fundamental peaks >10 at a periodicity of 1.6 µm (Fig. 2 C; Fig. S1; and Fig. S2 C). In contrast, 7% of Flag-RadΔCT cells were classified as displaying organized t-tubular expression. 22% showed FFT power over 10; however, notably, 0% of Flag-RadΔCT cells showed Flag-expression throughout the entire cell in contrast to 55% of Flag-Rad cells.

Proteins found in the junctional dyad, such as $Ca_V1.2$, show a periodic signal that repeats with the average murine t-tubular periodicity of 1.8 µm (Soeller and Cannell, 1999; Hong et al., 2010; Maleckar et al., 2017; Ito et al., 2019). The signal in Flag-Rad, but not in Flag-RadΔCT cardiomyocytes, qualitatively co-localizes with anti-$Ca_V1.2$ staining (Fig. 2 D). Taken together these data suggest that the Rad C-terminus is required for Rad localization to cardiomyocyte membrane domains in common with $Ca_V1.2$.

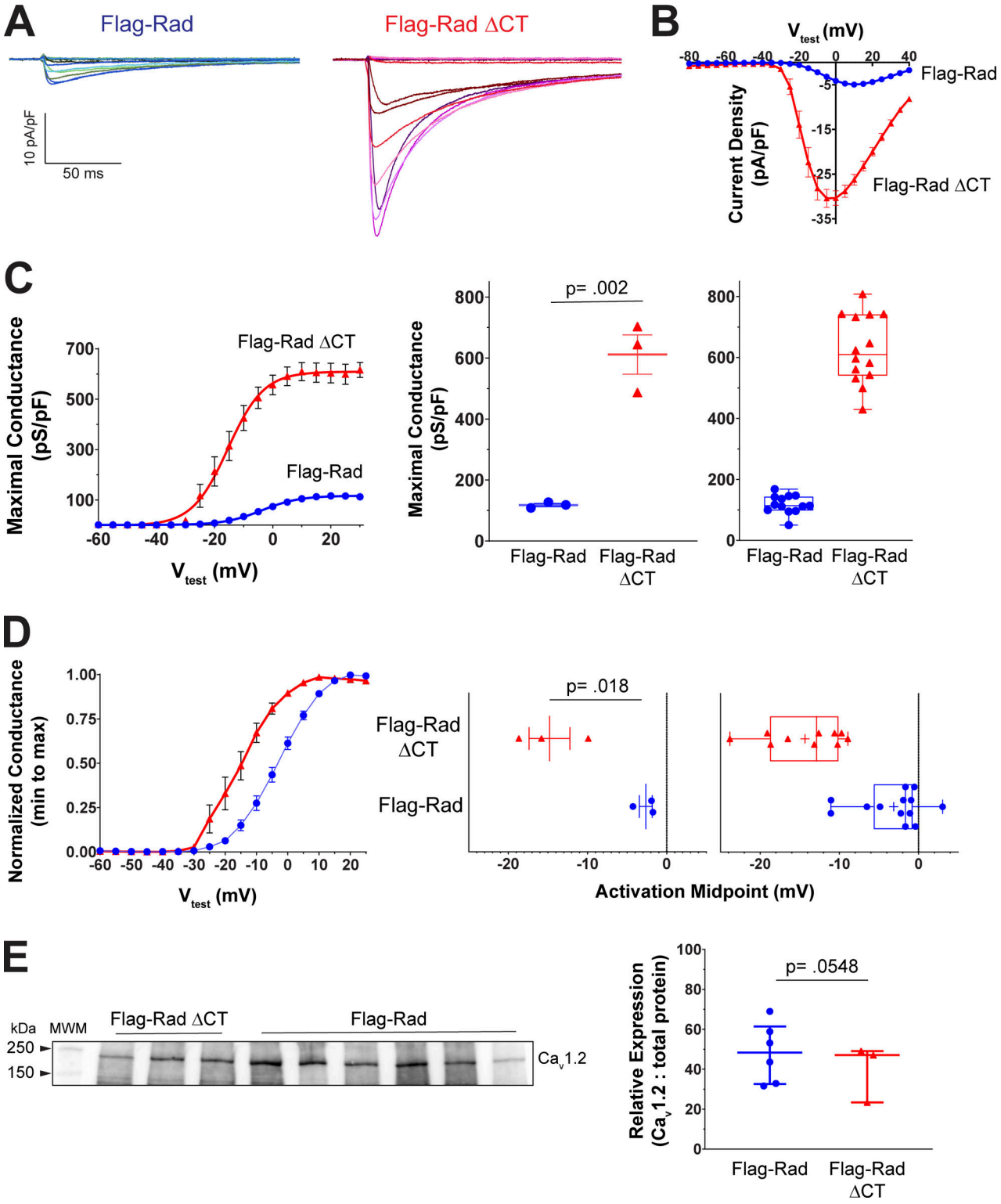

Figure 3. **Modulated $I_{Ca,L}$ in adult Flag-RadΔCT murine cardiomyocytes. (A)** Representative family of $I_{Ca,L}$ currents. Voltage protocol schematic above current traces. **(B)** Current density–voltage relationship for peak $I_{Ca,L}$ from Flag-Rad and Flag-RadΔCT ex vivo cardiomyocytes. **(C)** Conductance transforms of the current–voltage curve. Smooth curves are Boltzmann distribution fitted to data. Mean maximal conductance was significantly increased 5.2-fold in Flag-RadΔCT (614.8, 95% CI 528.4, 701.2) compared with Flag-Rad (118.0, 95% CI 30.7, 205.2) (estimated marginal means). Statistical significance was determined by a linear mixed model, nesting cells into the random factor mouse. Genotype as a main effect was significantly different (P = 0.002, F = 62.856). **(D)** To highlight the shift in activation midpoint, the conductance–voltage curves were normalized to maximum conductance. The mean activation midpoint was significantly shifted negatively at 11.3 mV in Flag-RadΔCT (−14.2, 95% CI −17.6, −10.9) relative to Flag-Rad (−3.0, 95% CI −5.9, 0.02) (estimated marginal means). Statistical significance was determined by a linear mixed model, nesting cells into the random factor mouse. Genotype as a main effect was significantly different (P = 0.018, F = 24.419). Mice are shown to the left and cells to the right. For mice, means and SEM are plotted; for cells, medians, and IQR. For Flag-Rad (*N* = 3 mice,

n = 13 cells); for Flag-RadΔCT (*N* = 3 mice, *n* = 14 cells). **(E)** Western blot for $Ca_V1.2$ expression in protein lysates from Flag-Rad and Flag-RadΔCT whole heart lysates. Median relative expression of $Ca_V1.2$ (normalized to total protein) was not significantly different (Mann–Whitney U test, P = 0.5476, U = 6). Source data are available for this figure: SourceData F3.

The loss of organized, t-tubular pattern expression of anti-Flag-Rad signal in Flag-RadΔCT could result from a general loss of dyad organization. To address this question, primary cardiomyocytes were stained for α-actinin. Cardiomyocytes from Flag-Rad and Flag-RadΔCT presented with highly structured order (Fig. S4 A). T-tubules were probed using live cell staining with di-8-ANEPPS. FFT produced a strong fundamental peak in the power spectra at ∼1.8 µm periodicity in cells of both genotypes, suggesting a regular transverse tubule network that was not significantly different between Flag-Rad and Flag-RadΔCT mice (Fig. S4 B). Brightfield microscopy of live cells demonstrated that both genotypes had mean resting sarcomere lengths of 1.9 µm, suggesting that the 1.6 µm periodicity derived from the anti-Flag cell immunocytochemistry is likely a fixation artifact and not representative of live cell resting sarcomere length (Fig. S4 C) or t-tubular periodicity (Fig. S4 B).

Deletion of the C-terminus tail of Rad resulted in modulated $I_{Ca,L}$ under basal conditions

Flag-RadΔCT showed reduced membrane localization suggesting that binding to $Ca_V\beta$ is alone insufficient to generate stable Rad:LTCC complexes, but it is unknown whether durable Rad interaction is required for Rad-mediated channel regulation. L-type channel complexes without Rad show modulated $I_{Ca,L}$ under basal conditions (Ahern et al., 2019). Fig. 3 A shows representative families of $I_{Ca,L}$ traces from cardiomyocytes isolated from Flag-Rad and Flag-RadΔCT hearts. The I(V) curve for Flag-RadΔCT shows increased peak current density compared with Flag-Rad (Fig. 3 B). Flag-RadΔCT showed a 5.2-fold increase in maximal conductance (Fig. 3 C) and a hyperpolarizing shift of activation midpoint (shifted −11 mV) compared to Flag-Rad (Fig. 3 D). Western blotting from whole hearts found no significant change in $Ca_V1.2$ expression between Flag-Rad and Flag-RadΔCT mice (Fig. 3 E).

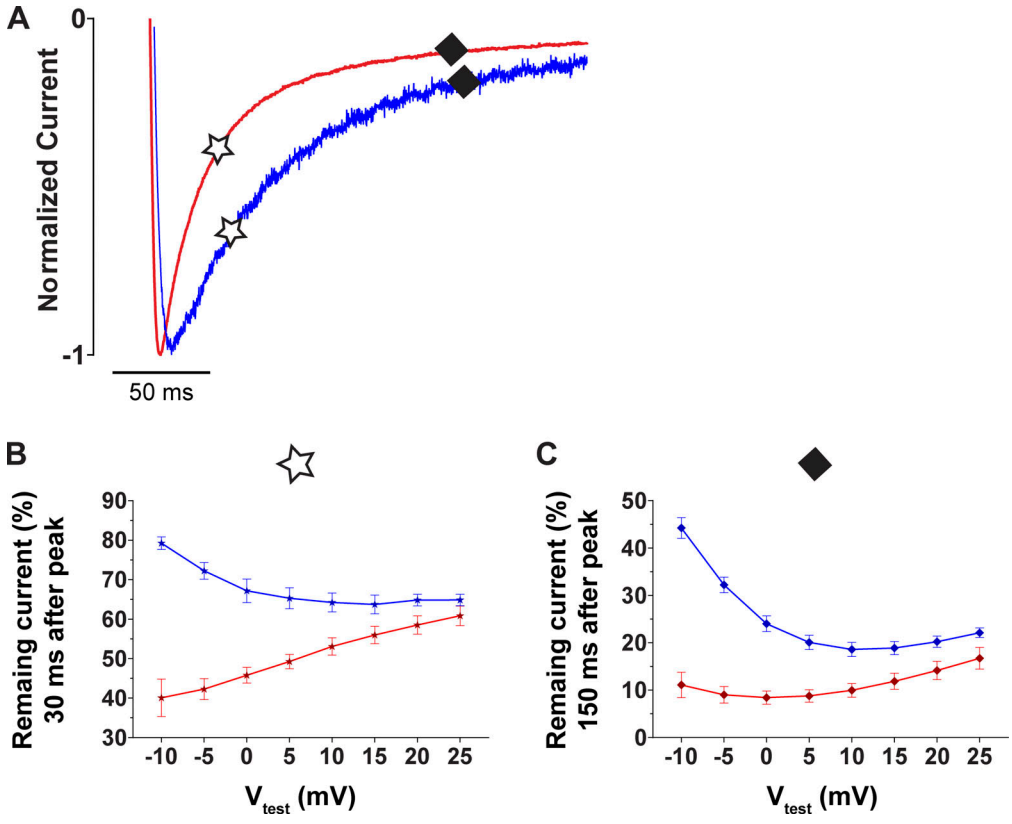

Figure 4. **Flag-RadΔCT cardiomyocytes display faster $I_{Ca,L}$ decay kinetics. (A)** Representative $I_{Ca,L}$ current recorded for V_{hold} = −80 mV stepped to V_{test} = 0 mV, normalized to maximum peak current to highlight kinetic differences between Flag-Rad and Flag-RadΔCT. Black stars indicate the remaining current 30 ms after the peak current; black diamonds, 150 ms after the peak current. **(B)** Percent remaining current 30 ms after peak. Flag-RadΔCT had significantly less remaining current/faster decay (linear mixed model; genotype P = 0.002, F = 55.5362; voltage P = 0.058, genotype × voltage P = 0.002, F = 109.422). The remaining current was on average reduced 25% in Flag-RadΔCT (51% remaining current) relative to Flag-Rad (68%). **(C)** Percent remaining current 150 ms after peak across various test potentials. Flag-RadΔCT had significantly less remaining current/faster decay (linear mixed model; genotype P = 0.001, F = 80.672; voltage P < 0.001; interaction P < 0.001, F = 81.684). The remaining current was on average reduced 55% in Flag-RadΔCT (11% remaining current) relative to Flag-Rad (25%). For Flag Rad (*N* = 3 mice, *n* = 13 cells); for Flag-RadΔCT (*N* = 3 mice, *n* = 14 cells). Means of mice with SEM shown. Data points of individual cells and individual mice are in Fig. S3.

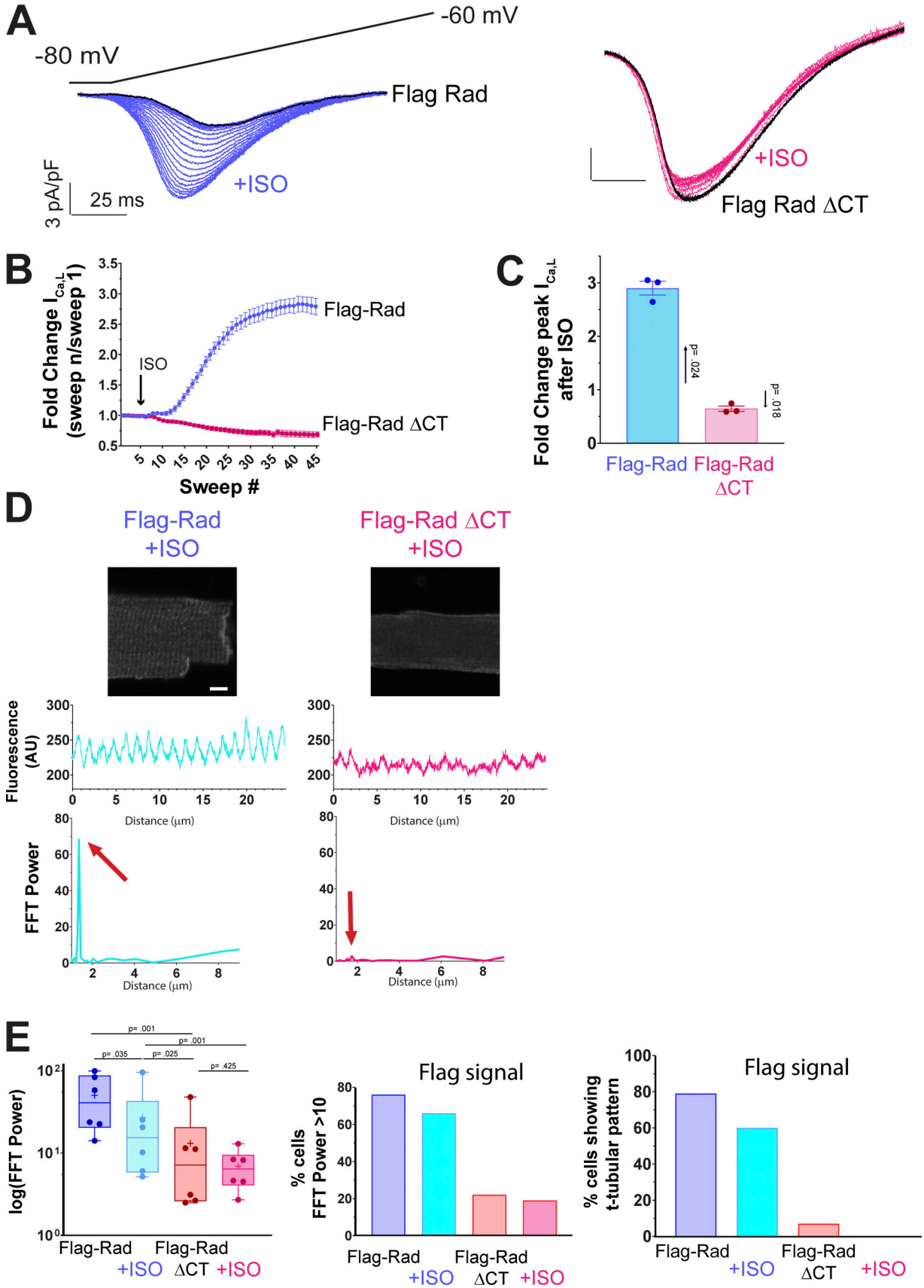

Figure 5. **Flag-Rad adult murine cardiomyocytes treated with β-adrenergic agonists show modulated $I_{Ca,L}$ that phenocopies untreated Flag-RadΔCT and reduced t-tubular expression. (A)** Flag-Rad cardiomyocytes with 300 nM β-adrenergic receptor agonist ISO show an increase of $I_{Ca,L}$. Black traces

(baseline). Cyan (Flag-Rad) and pink (Flag-RadΔCT) show sweeps after the addition of β-adrenergic receptor agonist. Ramp protocol (above current sweeps) repeated at 3 s inter-pulse interval. **(B)** Diary plot of fold change of mean peak $I_{Ca,L}$ recorded during continuous recordings (sweeps) relative to initial peak current of sweep 1. **(C)** The fold change in $I_{Ca,L}$ after application of ISO (after steady state was reached). $I_{Ca,L}$ of Flag-Rad cardiomyocytes significantly increased 2.9-fold from a mean −2.8 (95% CI, −3.5, −2.2) to −8.2 (95% CI, −10.0, −6.4) pA/pF (linear mixed model, ISO treatment P = 0.024, F = 51.001, *N* = 3 mice, *n* = 13 cells). $I_{Ca,L}$ of Flag-RadΔCT cardiomyocytes significantly changed 0.7-fold from mean −11.1 (95% CI, −13.1, −9.1) to −7.5 pA/pF (linear mixed model, ISO treatment P = 0.018, F = 6.491, *N* = 3 mice, *n* = 12 cells). **(D)** Confocal micrographs of adult cardiomyocytes treated with 1 µM β-adrenergic receptor agonist ISO from Flag-Rad or Flag-RadΔCT mice. Scale bar, 5 µm. Fluorescence intensity profiles of regions of interest from the representative images and their FFT power spectrums. **(E)** FFT data of untreated cardiomyocytes (data from Fig. 2) were analyzed together with ISO-treated cells to consider for both genotype and drug treatment as fixed factors with a linear mixed model (nesting cells into mice and accounting for cells untreated or treated originated from the same mouse). Data of untreated cells shown in Fig. 2 is repeated for clarity. The drug treatment main effect (P = 0.032, F = 5.147) was significant and, as reported in Fig. 2, the genotype main effect was significant (P = 0.002, F = 16.502); the interaction term was not (P = 0.255, F = 1.360). The FFT peak power median of Flag-Rad treated with β-adrenergic receptor agonist 15.4 (IQR: 5.8-42.9; *N* = 6 mice, *n* = 30 cells, 64 images) was significantly reduced 62% of untreated Flag-Rad 40.9 (IQR: 20.4–87.6) but still significantly 115 and 140% higher than untreated Flag-RadΔCT 7.1 (IQR: 2.6–20.6) and ISO-treated Flag-RadΔCT 6.4 (IQR: 4.1–9.5; *N* = 6 mice, 33 cells, 62 images). The P values of pairwise comparisons were corrected for multiple comparisons using Holm adjustment of estimated marginal means. 76% of Flag-Rad and 66% of Flag-Rad + ISO whereas 22 and 19% of Flag-RadΔCT ± ISO had a fundamental peak with power >10. Blinded researchers classified 79 and 60% of Flag-Rad ± ISO and 7 and 0% of Flag-RadΔCT ± ISO cells as having organized t-tubular expression in at least one region of the cell. Two to four technical replicate images' FFT power were averaged per cell. The total sampling size was 12 mice, 143 cells, and 311 images.

$I_{Ca,L}$ in cardiomyocytes isolated from Flag-RadΔCT hearts exhibit enhanced decay kinetics relative to $I_{Ca,L}$ from Flag-Rad myocytes (Fig. 4). Representative traces normalized to maximum current and superimposed show that Flag-RadΔCT myocytes display faster current decay than that of Flag-Rad (Fig. 4 A). The early component of decay, largely reflecting Ca^{2+}-dependent inactivation, was analyzed by assessing the percentage of remaining current 30 ms after peak current. Flag-RadΔCT $I_{Ca,L}$ showed a significant reduction in mean remaining current (faster decay) across multiple voltages (linear mixed model; genotype P = 0.002, F = 55.5362) (Fig. 4 B and Fig. S3 A). The difference between Flag-RadΔCT and Flag-Rad decay at 30 ms diminished for a more positive V_{test} as expected for Ca^{2+}-dependent inactivation (Ahern et al., 2021). The late $I_{Ca,L}$ decay was quantified by measuring the percentage of remaining current 150 ms after peak current. Flag-RadΔCT again showed a significant reduction in mean remaining current (faster decay) across multiple voltages (linear mixed model; genotype P = 0.001, F = 80.672) (Fig. 4 C and Fig. S3 B). Taken together, these data suggest that cardiomyocytes expressing Flag-RadΔCT have modulated $I_{Ca,L}$ under basal conditions similar to that of $I_{Ca,L}$ seen following complete genetic Rad knockout or in WT cardiomyocytes under acute β-adrenergic receptor agonist stimulation (Manning et al., 2013; Ahern et al., 2019, 2021).

Acute β-adrenergic receptor agonist stimulation of Flag-Rad cardiomyocytes showed modulated $I_{Ca,L}$ phenocopying untreated Flag-RadΔCT

We next tested whether the modulated $I_{Ca,L}$ observed in Flag-RadΔCT cardiomyocytes under basal conditions recapitulates that of β-adrenergic receptor modulated $I_{Ca,L}$. Flag-Rad cardiomyocytes were acutely treated with ISO. To capture the acute, real-time change, the experiment was performed in a paired fashion with a continuous ramp protocol (Fig. 5, A–C). ISO increased Flag Rad $I_{Ca,L}$ significantly by a mean of threefold with modulated Flag-Rad $I_{Ca,L}$ resembling that observed in untreated Flag-RadΔCT cardiomyocytes. In contrast to Flag-Rad, ISO stimulation did not increase $I_{Ca,L}$ in Flag-RadΔCT cardiomyocytes (Fig. 5, A–C).

Flag-Rad staining pattern after β-adrenergic receptor agonist treatment

Recent studies suggested that PKA phosphorylation of Rad releases L-type calcium channel inhibition by loss of Rad within close proximity to $Ca_V1.2$ and $Ca_V\beta$ (Liu et al., 2020; Papa et al., 2022); therefore, we assessed the localization pattern of Rad after β-adrenergic receptor agonist administration. As in Fig. 2, confocal micrographs from Flag-Rad cardiomyocytes without, or 3 min following ISO stimulation, were analyzed with FFT (Fig. 5 D). The ISO treatment main effect was significant (P = 0.032, F = 5.147) and the median FFT power of Flag-Rad cardiomyocytes treated with ISO was significantly reduced by 62% relative to untreated Flag-Rad myocytes; however, 66% of ISO-treated Flag-Rad cardiomyocytes still showed FFT power over 10, only 10% less than untreated Flag-Rad (Fig. 5 E and Fig. S2). Blinded researchers classified less ISO-treated Flag-Rad cells as having organized t-tubular expression: 60% ISO-treated Flag-Rad versus 79% untreated.

As reported in Fig. 2, which focused on the genotype difference, the main effect of genotype (P = 0.002, F = 16.502) was significant considering all 12 mice and 311 cells ±ISO. Flag-Rad and ISO-treated Flag-Rad cardiomyocytes had mouse median FFT powers in the double-digits while both medians of Flag-RadΔCT ±ISO groups were <10 (Fig. 5 E and Fig. S2 C). Flag-Rad cardiomyocytes untreated and ISO-treated had three- to fourfold greater percentages of cells with fundamental FFT power peaks >10.

Similarly, blinded researchers classified 79 and 60% of Flag-Rad ± ISO and 7 and 0% of Flag-RadΔCT ± ISO cells as having organized t-tubular expression in at least one region of the cell.

Flag-RadΔCT shows elevated basal heart function

We previously showed that constitutive, global Rad-knockout phenocopies β-AR stimulation at multiple levels, from $I_{Ca,L}$ to in vivo heart function. We next performed an ISO stress echocardiography test in Flag-Rad and Flag-ΔCT mice. The left ventricular (LV) ejection fraction was significantly lower in Flag-Rad compared with Flag-RadΔCT in the basal condition (Fig. 6, A and B). Acute ISO resulted in a significant increase of

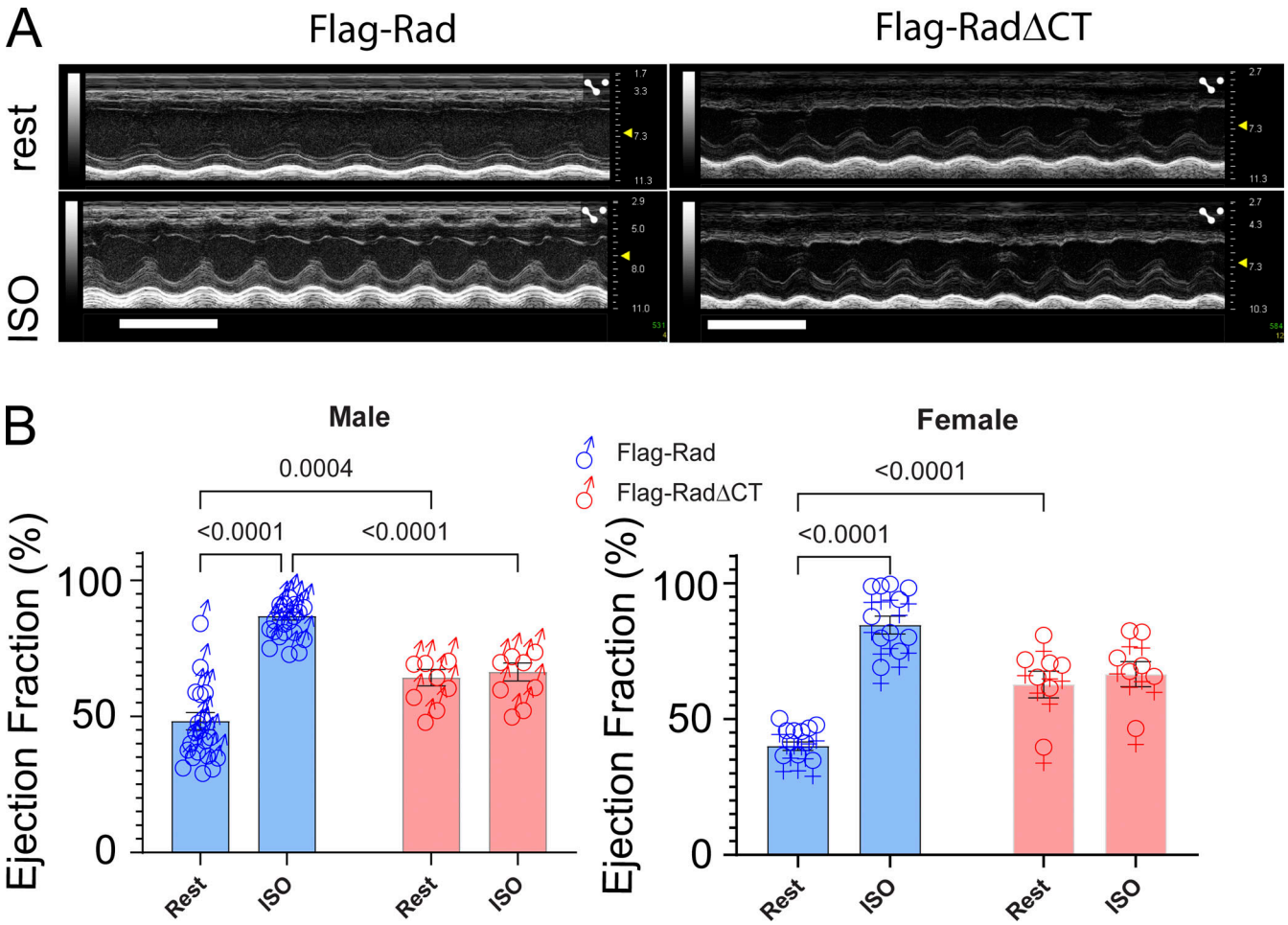

Figure 6. **Flag-RadΔCT hearts show elevated function under basal conditions**. Heart function was evaluated by echocardiography. **(A)** Representative M-mode recordings from Flag-Rad (left) and Flag-RadΔCT mice (right). The upper panel shows recording prior to ISO injection and lower panel shows same mice 1–3-min after ISO injection. **(B)** Ejection fraction (%) for male (left) and female mice (right) was significantly different between genotypes in the basal condition and significantly different in Flag-RAD after ISO. Sex as a main effect was not statistically significant (three-way repeated measures ANOVA, F = 1.050, P = 0.3113). Repeated measures two-way ANOVA's were performed considering repeated measures basal versus acute ISO treatment and genotype (male: treatment F = 78.13, P < 0.0001; genotype F = 0.3790, P = 0.5435; interaction F = 62.75 P < 0.0001) (female: treatment F = 134.1, P < 0.0001; genotype F = 0.2705, P = 0.6101; interaction F = 95.04, P < 0.0001). Scale bar = 200 ms.

ejection fraction in Flag-Rad but not Flag-RadΔCT (Fig. 6, A and B). Similar results were obtained from male and female mice (Fig. 6 and Table 1) with the exception that LV mass was greater in male Flag-Rad (Table 1). These results suggest that Flag-RadΔCT heart function phenocopies that of myocardial Rad knockout.

Discussion

The major finding of this study is that the polybasic C-terminus of Rad is required for membrane localization and for L-type calcium channel regulation in cardiomyocytes. To preserve native protein complexes, we engineered a transgenic mouse model containing an N-terminal Flag epitope, allowing the subcellular distribution of Rad protein to be assessed for the first time at native levels of expression using microscopy. We now report that Rad is enriched in a striated pattern in adult ventricular cardiomyocytes, consistent with the distribution of $Ca_V1.2$, the main pore-forming subunit of the cardiac L-type calcium channel. In contrast, truncation of the C-terminal results in a significantly reduced striated cellular distribution of Flag-RadΔCT, with a corresponding loss in correlation with $Ca_V1.2$ staining. In cardiomyocytes expressing Flag-RadΔCT, $I_{Ca,L}$ is modulated under baseline conditions consistent with properties of myocytes genetically deleted for Rad (Manning et al., 2013; Ahern et al., 2019, 2021), or those expressing full-length Rad following β-adrenergic receptor modulation.

The RGK-conserved C-terminus is crucial for membrane targeting

Several independent lines of evidence now support the importance of the evolutionarily conserved C-terminal domain in the biological function of all RGK subfamily G-proteins (Puhl et al., 2014). Heo and colleagues (Heo et al, 2006) first demonstrated that membrane targeting by the isolated RGK C-terminal membrane targeting domain involves the interaction of conserved polybasic amino acids with negatively charged phosphatidylinositol

Table 1. **Echocardiography acute β-AR stress test**

Males						
		Flag-Rad +ISO	**(*N* = 20) P**		**Flag-RadΔCT +ISO**	**(*N* = 8) P**
HR	434 ± 19	575 ± 11	$<10^{-4}$	496 ± 21	560 ± 17	0.02
EF (%)	48.2 ± 3.1	86.8 ± 1.4	$<10^{-4}$	64.2 ± 3.0	66.3 ± 3.3	0.963
LVID;d (mm)	4.50 ± 0.15	3.26 ± 0.09	$<10^{-4}$	3.59 ± 0.10	3.16 ± 0.14	0.060
LVAW;d (mm)	0.86 ± 0.02	1.16 ± 0.02	$<10^{-4}$	1.07 ± 0.08	1.05 ± 0.11	0.988
LVPW;d (mm)	0.76 ± 0.04	1.05 ± 0.04	$<10^{-4}$	0.95 ± 0.04	1.04 ± 0.07	0.525
LVmass (mg)	146 ± 8*			130 ± 11		0.468
Females						
		Flag-Rad	**(*N* = 11)**		**Flag-RadΔCT**	**(*N* = 7)**
		+ISO	**P**		**+ISO**	**P**
HR	408 ± 19	525 ± 10	$<10^{-4}$	528 ± 13	577 ± 21	0.14
EF (%)	40.0 ± 1.5	84.6 ± 3.3	$<10^{-4}$	62.7 ± 4.9	66.5 ± 4.6	0.792
LVID;d (mm)	4.48 ± 0.14	3.32 ± 0.12	$<10^{-4}$	3.50 ± 0.15	3.34 ± 0.21	0.693
LVAW;d (mm)	0.66 ± 0.03	0.97 ± 0.03	$<10^{-4}$	1.07 ± 0.07	1.01 ± 0.06	0.700
LVPW;d (mm)	0.59 ± 0.05	0.97 ± 0.05	$<10^{-4}$	0.86 ± 0.07	0.91 ± 0.06	0.936
LVmass (mg)	103 ± 6*			123 ± 16		0.304

Means ± SEM. Echocardiography parameters of Flag-Rad mice but not Flag-RadΔCT show significant changes after acute ISO administration. Pairwise comparison P values of before/after ISO in each genotype were corrected using Sidak's multiple comparison test. For LVmass in the basal condition, a two-way ANOVA considering sex and genotype, there was a significant sex (F = 4.722, P = 0.0355) but not genotype (F = 0.1125, P = 0.7390) main effect or interaction (F = 3.228, P = 0.0796). The pairwise comparisons are corrected for multiple comparisons using Sidak's adjustment. HR = heart rate, EF = ejection fraction, LVID;d left ventricular internal diameter; diastolic, LVAW;d left ventricular anterior wall; diastolic, LVPW;d left ventricular posterior wall; diastolic.

4,5-bisphosphate and phosphatidylinositol 3,4,5-trisphosphate lipids. Studies in immortalized cell lines support the importance of this conserved domain as an intact C-terminal domain is necessary for Rad- and Rem-dependent $I_{Ca,L}$ inhibition and plasma membrane association (Finlin et al., 2003; Correll et al., 2007). The C-terminus of Rem and Rem2 is required for phosphatidyl-inositol lipids—RGK association (Correll et al., 2007, 2008a). Furthermore, C-terminal Rem and Rem2 deletion mutants retain their ability to bind $Ca_V\beta$ subunits but fail to inhibit $I_{Ca,L}$, indicating that $Ca_V\beta$ subunit binding is alone not sufficient for Rem/Rem2-dependent LTCC regulation (Correll et al., 2007, 2008a). However, fusion of the CAAX membrane targeting motif from Ras proteins to C-terminal truncated Rem (Correll et al., 2007) restored membrane localization and LTCC regulation (Correll JBC 2007), suggesting that $Ca_V\beta$ binding and membrane localization are independent events required for RGK-dependent LTCC regulation. Consistent with results in heterologous cell models, we find that Flag-tagged Rad at endogenous expression levels is localized in repeating t-tubular pattern that colocalizes with $Ca_V1.2$ staining in cardiomyocytes and that this subcellular distribution depends upon the presence of an intact Rad C-terminal membrane targeting domain.

We used in silico tools to graphically represent the consequence of deleting the Rad C-terminus. Amphipathic α-helixes are common secondary structure motifs that can mediate weak, reversible binding of plasma membranes (Hatzakis et al., 2009). AlphaFold predicts in Rad an amphipathic α-helix from amino acids 273–288 (Fig. 7 A) (Jumper et al., 2021). In this model, helix 8 of Rad contains six Lys or Arg residues that alternate coordinately with hydrophobic residues. AlphaFold (Jumper et al., 2021; Mirdita et al., 2022) was used to generate a model for RadΔCT (Fig. 7, A and B; and Video 3). The PPM3.0 computational tool for predicting membrane interaction was used to calculate the interaction of both proteins with a mammalian plasma membrane (Lomize et al., 2012, 2022) (Fig. 7 A). The predicted $\Delta G_{transfer}$ for Flag-RadΔCT from water to a lipid bilayer was reduced twofold from −7.3 to −2.8 kcal/mol (Fig. 7 C), a change consistent with a loss of membrane association (Fig. 7). In summary, this analysis strongly suggests that the C-terminal domain of Rad is essential for membrane localization.

β-Adrenergic receptor activation and Rad localization

Regulation of $I_{Ca,L}$ downstream of activated PKA involves multiple proteins within the L-type calcium channel complex. Our early findings showed that the absence of Rad results in a tonic-modulated $I_{Ca,L}$ in sinoatrial nodal (Levitan et al., 2021) and ventricular cardiomyocytes (Ahern et al., 2019a), even in the absence of β1- and β2-adrenergic receptor expression (Ahern et al., 2021). We now show that Rad retains membrane localization with acute β-AR stimulation, albeit with significantly reduced power. A proximity proteomic study suggested that Rad was lost from the proximal LTCC microenvironment following β-AR stimulation (Liu et al., 2020; Papa et al., 2022). Acute β-AR stimulation promotes recycling/reinsertion of $Ca_V1.2$ in a Rab4a- and Rab11a-dependent fashion (Del Villar et al., 2021). Future

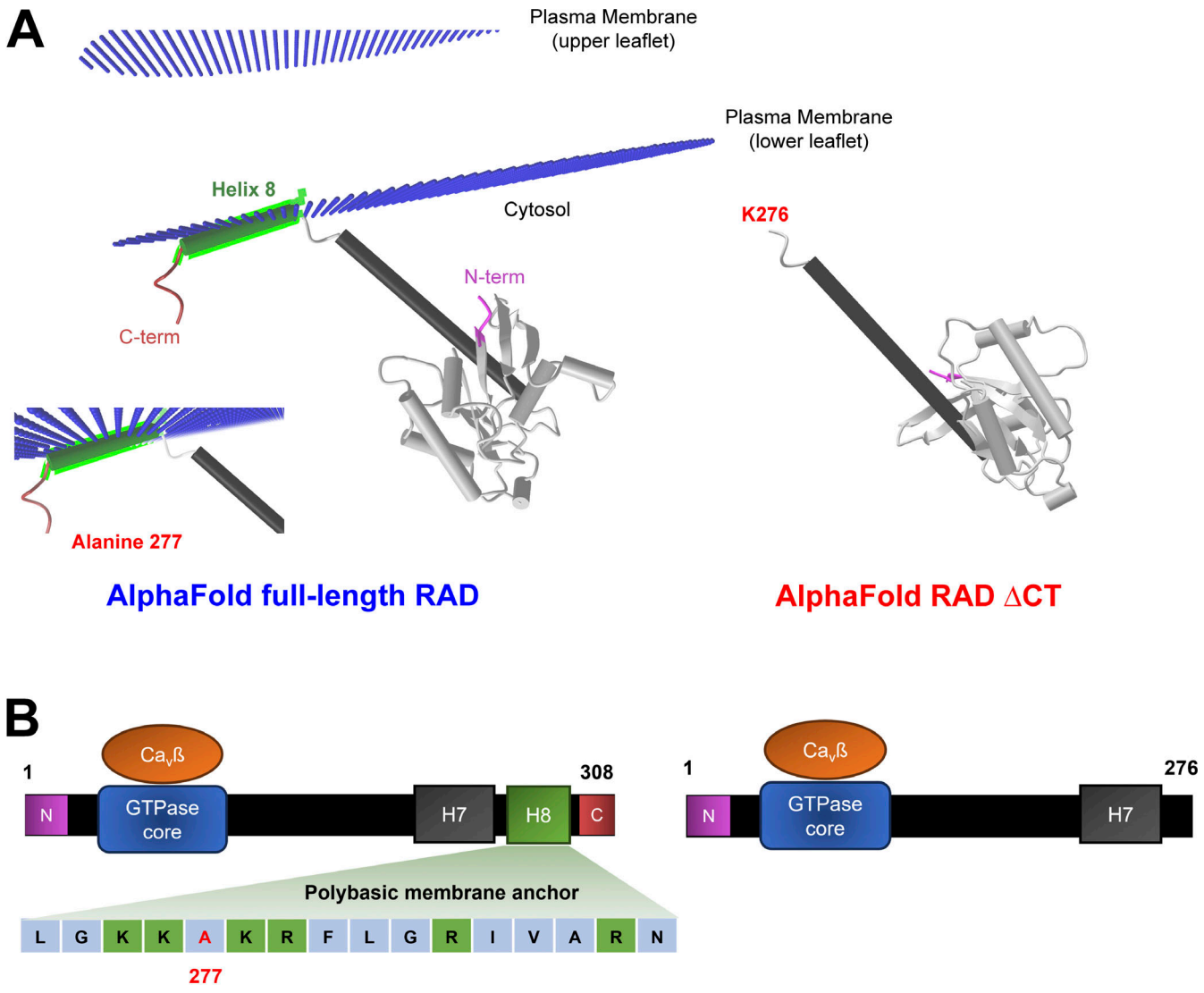

C

Computational modeling interaction with membrane (PPM 3.0)	Full-length RAD (1-308)	RAD ΔCT (1-276)
$\Delta G_{transfer}$ of protein from water to lipid bilayer (kcal/mol)	-7.3	-2.8†
Membrane Embedded residues	274-275, 278, 281-282,285,289	152, 154

Figure 7. **Computational modeling predicts a basic amphipathic α-helix motif in the C-terminus anchors Rad to the plasma membrane. (A)** AlphaFold prediction of *M. musculus* Rad full-length (Uniprot accession no. O88667) was input to the PPM 3.0 web server tool for computational modeling of Rad with a mammalian membrane. The inset image focuses on the predicted embedded residues that are amino acids in the predicted helix 8 (H8) and highlights the alanine which was replaced with a stop codon in the Flag-RadΔCT mouse model. AlphaFold was then used to predict a structure for RadΔCT. Modelling RadΔCT (1–276) with PPM 3.0 predicts low probability of membrane interaction. **(B)** Abbreviated protein schematic of full length Rad and RadΔCT. The GTPase core is shown with its putative interaction with the L-type calcium channel $Ca_V\beta$ subunit. The amino acids of the predicted amphipathic α-helix basic residues are highlighted in green. Helices 7 (black) and 8 (green) correspond to the colored H7 and H8 in the Rad proteins in A. **(C)** Tabular results of PPM 3.0 predictions. Full-length Rad $\Delta G_{transfer}$ was increased 160% relative to RadΔCT. The RadΔCT $\Delta G_{transfer}$ of −2.8 kcal/mol is relatively low, suggesting a low probability for hydrophobic surfaces involved in protein–membrane interactions. The predicted residues (152 and 154) for RadΔCT reside in the GTPase core that is known to interact with $Ca_V\beta$.

work will be needed to address whether Rad participates in early endosome-mediated L-type calcium channel recycling (Ito et al., 2019; Westhoff and Dixon, 2021). In *Xenopus* oocytes, multiple proteins can be expressed approximating tunable stoichiometric ratios (Weiss et al., 2013). Interestingly, Rad-dependent and Rad-independent PKA regulation of $I_{Ca,L}$ was discovered (Katz et al., 2021). Recent work suggests added complexity of PKA regulation of $I_{Ca,L}$ arises from multiprotein interactions including tripartite interactions of PKA catalytic subunits with the C-termini of $Ca_V1.2$. In this vein, it is worth noting that evidence exists for Rem—$Ca_V1.2$-proximal–C-terminal interaction in a Ca^{2+}-calmodulin-dependent fashion, thus raising the specter of pentapartite interactions conferring modulation of $I_{Ca,L}$.

Regulation of Rad's interaction with the L-type calcium channel

We previously reported that Rad slows $I_{Ca,L}$ kinetics in cardiomyocytes (Ahern et al., 2021). The loss of Rad-regulation of the LTCC increases peak trigger Ca^{2+}, and yet, the faster decay kinetics precludes elevation of late $I_{Ca,L}$. As shown previously by others, late $I_{Ca,L}$ is proarrhythmic (Madhvani et al., 2011, 2015). Previous work suggests that disruption of the Rad:CaVβ interaction could be inotropic by increasing Ca^{2+} entry. In this context, it is interesting that deletion of the Rad C-terminus phenocopied Rad-deletion kinetics. This suggests a new therapeutic direction for targeting Rad–C-terminal interaction with the plasma membrane (PIP lipids) as a means for boosting trigger Ca^{2+} for excitation–contraction coupling without necessarily promoting pathologies related to Ca^{2+} overload caused by overactive L-type Ca^{2+} channels.

In conclusion, we show that full-length Flag Rad is expressed in a regular, striated subcellular distribution in cardiomyocytes consistent with a t-tubule expression pattern and localization to the junctional dyad. Deletion of the C-terminus ablates the plasma membrane targeting of Rad in cardiomyocytes, resulting in similar results to that in earlier heterologous expression system studies, showing a lack of membrane expression and instead nuclear and diffuse cytosolic signal. Flag-RadΔCT $I_{Ca,L}$ is modulated under basal conditions similarly to that of $I_{Ca,L}$ of β-AR–treated cardiomyocytes, both recapitulating the increased open probability, negative shift of activation midpoint, and hastened inactivation observed in β-adrenergic receptor modulation of the L-type calcium channel. With no C-terminus to anchor it to the membrane in t-tubules, we observed no evidence of a Rad interaction with $Ca_V1.2$; thus, a similar phenotype to that of Rad knockout occurs (Manning et al., 2013; Ahern et al., 2019, 2021).

Online supplemental material

Fig. S1 contains 16 confocal micrographs of fixed adult murine ventricular cardiomyocytes immunostained with anti-Flag antibody in addition to control micrographs (e.g., a Rad knockout mouse, a no primary control). Fig. S2 contains 16 confocal micrographs similarly treated except the cells were incubated with 1 µM ISO for 3 min to supplement Fig. 5 D's two representative images. Fig. S2, B and C show the non-log_{10}-transformed mice means, and log_{10} and non-transformed individual cell data is shown in Fig. S2 C and Fig. 5 E. Fig. S3 and Fig. S4 show averaged data with individual mouse and cell data and the 95% confidence intervals of the genotype differences at each V_{test}. Fig. S4 displays microscopy assessing t-tubule integrity and quantitates resting sarcomere length in live cardiomyocytes. Video 1 SR SIM of maximal intensity projection (multiple z-slices) of Flag-Rad stained with Flag antibody. Scale x = 32.9 µm; y = 32.9 µm; z = 4.1 µm. Video 2 SR SIM of maximal intensity projection (multiple z-slices) of Flag-RadΔCT stained with Flag antibody. Scale x = 32.9 µm; y = 32.9 µm; z = 4.9 µm. Video 3 Alphafold full-length Rad (Uniprot accession no. O88667) PPM 3.0 computational model of interaction with the plasma membrane.

Data availability

The data are available from the corresponding author upon reasonable request.

Acknowledgments

David A. Eisner served as editor.

This research was funded by an American Heart Association pre-doctoral fellowship to B.M. Ahern (19PRE34380909), NIH/National Heart, Lung and Blood Institute grant HL166280, and Department of Defense grant W81WXH-20-1-0418.

Author contributions: G. Elmore: Conceptualization, Data curation, Formal analysis, Investigation, Methodology, Software, Validation, Visualization, Writing—original draft, Writing—review & editing, B.M. Ahern: Conceptualization, Data curation, Formal analysis, Funding acquisition, Investigation, Visualization, Writing—review & editing, N.M. McVay: Formal analysis, Investigation, Writing—review & editing, K.W. Barker: Formal analysis, Investigation, Methodology, Validation, Visualization, Writing—original draft, S.S. Lohano: Data curation, Formal analysis, Investigation, Visualization, N. Ali: Data curation, Formal analysis, Investigation, Methodology, Writing—review & editing, A. Sebastian: Investigation, Methodology, Resources, Writing—review & editing, D.A. Andres: Conceptualization, Funding acquisition, Investigation, Methodology, Supervision, Validation, Writing—review & editing, J. Satin: Conceptualization, Data curation, Formal analysis, Funding acquisition, Methodology, Project administration, Resources, Supervision, Validation, Visualization, Writing—original draft, Writing—review & editing, B.M. Levitan: Data curation, Formal analysis, Investigation.

Disclosures: The authors declare no competing interests exist.

Submitted: 5 December 2023
Revised: 17 May 2024
Accepted: 26 June 2024

References

Ahern, B.M., B.M. Levitan, S. Veeranki, M. Shah, N. Ali, A. Sebastian, W. Su, M.C. Gong, J. Li, J.E. Stelzer, et al. 2019. Myocardial-restricted ablation of the GTPase RAD results in a pro-adaptive heart response in mice. *J. Biol. Chem.* 294:10913–10927. https://doi.org/10.1074/jbc.RA119.008782

Ahern, B.M., A. Sebastian, B.M. Levitan, J. Goh, D.A. Andres, and J. Satin. 2021. L-type channel inactivation balances the increased peak calcium

current due to absence of Rad in cardiomyocytes. *J. Gen. Physiol.* 153: e202012854. https://doi.org/10.1085/jgp.202012854

Béguin, P., K. Nagashima, T. Gonoi, T. Shibasaki, K. Takahashi, Y. Kashima, N. Ozaki, K. Geering, T. Iwanaga, and S. Seino. 2001. Regulation of Ca2+ channel expression at the cell surface by the small G-protein kir/Gem. *Nature*. 411:701–706. https://doi.org/10.1038/35079621

Béguin, P., R.N. Mahalakshmi, K. Nagashima, D.H. Cher, A. Takahashi, Y. Yamada, Y. Seino, and W. Hunziker. 2005. 14-3-3 and calmodulin control subcellular distribution of Kir/Gem and its regulation of cell shape and calcium channel activity. *J. Cell Sci.* 118:1923–1934. https://doi.org/10.1242/jcs.02321

Béguin, P., R.N. Mahalakshmi, K. Nagashima, D.H. Cher, H. Ikeda, Y. Yamada, Y. Seino, and W. Hunziker. 2006. Nuclear sequestration of beta-subunits by Rad and Rem is controlled by 14-3-3 and calmodulin and reveals a novel mechanism for Ca2+ channel regulation. *J. Mol. Biol.* 355: 34–46. https://doi.org/10.1016/j.jmb.2005.10.013

Bers, D.M. 2002. Cardiac excitation-contraction coupling. *Nature*. 415: 198–205. https://doi.org/10.1038/415198a

Bers, D.M. 2008. Calcium cycling and signaling in cardiac myocytes. *Annu. Rev. Physiol.* 70:23–49. https://doi.org/10.1146/annurev.physiol.70.113006.100455

Chen, H., H.L. Puhl III, S.L. Niu, D.C. Mitchell, and S.R. Ikeda. 2005. Expression of Rem2, an RGK family small GTPase, reduces N-type calcium current without affecting channel surface density. *J. Neurosci.* 25: 9762–9772. https://doi.org/10.1523/JNEUROSCI.3111-05.2005

Correll, R.N., C. Pang, B.S. Finlin, A.M. Dailey, J. Satin, and D.A. Andres. 2007. Plasma membrane targeting is essential for Rem-mediated Ca2+ channel inhibition. *J. Biol. Chem.* 282:28431–28440. https://doi.org/10.1074/jbc.M706176200

Correll, R.N., G.J. Botzet, J. Satin, D.A. Andres, and B.S. Finlin. 2008a. Analysis of the Rem2 - voltage dependant calcium channel beta subunit interaction and Rem2 interaction with phosphorylated phosphatidylinositide lipids. *Cell. Signal.* 20:400–408. https://doi.org/10.1016/j.cellsig.2007.10.029

Correll, R.N., C. Pang, D.M. Niedowicz, B.S. Finlin, and D.A. Andres. 2008b. The RGK family of GTP-binding proteins: Regulators of voltage-dependent calcium channels and cytoskeleton remodeling. *Cell. Signal.* 20:292–300. https://doi.org/10.1016/j.cellsig.2007.10.028

Del Villar, S.G., T.L. Voelker, M. Westhoff, G.R. Reddy, H.C. Spooner, M.F. Navedo, E.J. Dickson, and R.E. Dixon. 2021. β-Adrenergic control of sarcolemmal $Ca_V1.2$ abundance by small GTPase Rab proteins. *Proc. Natl. Acad. Sci. USA*. 118:118. https://doi.org/10.1073/pnas.2017937118

Finlin, B.S., S.M. Crump, J. Satin, and D.A. Andres. 2003. Regulation of voltage-gated calcium channel activity by the Rem and Rad GTPases. *Proc. Natl. Acad. Sci. USA*. 100:14469–14474. https://doi.org/10.1073/pnas.2437756100

Guo, A., and L.S. Song. 2014. AutoTT: Automated detection and analysis of T-tubule architecture in cardiomyocytes. *Biophys. J.* 106:2729–2736. https://doi.org/10.1016/j.bpj.2014.05.013

Hatzakis, N.S., V.K. Bhatia, J. Larsen, K.L. Madsen, P.Y. Bolinger, A.H. Kunding, J. Castillo, U. Gether, P. Hedegård, and D. Stamou. 2009. How curved membranes recruit amphipathic helices and protein anchoring motifs. *Nat. Chem. Biol.* 5:835–841. https://doi.org/10.1038/nchembio.213

Heo, W.D., T. Inoue, W.S. Park, M.L. Kim, B.O. Park, T.J. Wandless, and T. Meyer. 2006. $PI(3,4,5)P_3$ and $PI(4,5)P_2$ lipids target proteins with polybasic clusters to the plasma membrane. *Science*. 314:1458–1461. https://doi.org/10.1126/science.1134389

Hong, T.-T., J.W. Smyth, D. Gao, K.Y. Chu, J.M. Vogan, T.S. Fong, B.C. Jensen, H.M. Colecraft, and R.M. Shaw. 2010. BIN1 localizes the L-type calcium channel to cardiac T-tubules. *PLoS Biol.* 8:e1000312. https://doi.org/10.1371/journal.pbio.1000312

Ito, D.W., K.I. Hannigan, D. Ghosh, B. Xu, S.G. Del Villar, Y.K. Xiang, E.J. Dickson, M.F. Navedo, and R.E. Dixon. 2019. β-adrenergic-mediated dynamic augmentation of sarcolemmal Ca_V 1.2 clustering and co-operativity in ventricular myocytes. *J. Physiol.* 597:2139–2162. https://doi.org/10.1113/JP277283

JASP Team. 2024. JASP (version 0.18.3) [Computer software]. https://jasp-stats.org/. Accessed July 10, 2024.

Jumper, J., R. Evans, A. Pritzel, T. Green, M. Figurnov, O. Ronneberger, K. Tunyasuvunakool, R. Bates, A. Žídek, A. Potapenko, et al. 2021. Highly accurate protein structure prediction with AlphaFold. *Nature*. 596: 583–589. https://doi.org/10.1038/s41586-021-03819-2

Katz, M., S. Subramaniam, O. Chomsky-Hecht, V. Tsemakhovich, V. Flockerzi, E. Klussmann, J.A. Hirsch, S. Weiss, and N. Dascal. 2021. Reconstitution of β-adrenergic regulation of $Ca_V1.2$: Rad-dependent and Rad-independent protein kinase A mechanisms. *Proc. Natl. Acad. Sci. USA*. 118:e2100021118. https://doi.org/10.1073/pnas.2100021118

Levitan, B.M., B.M. Ahern, A. Aloysius, L. Brown, Y. Wen, D.A. Andres, and J. Satin. 2021. Rad-GTPase contributes to heart rate via L-type calcium channel regulation. *J. Mol. Cell. Cardiol.* 154:60–69. https://doi.org/10.1016/j.yjmcc.2021.01.005

Liu, G., A. Papa, A.N. Katchman, S.I. Zakharov, D. Roybal, J.A. Hennessey, J. Kushner, L. Yang, B.-X. Chen, A. Kushnir, et al. 2020. Mechanism of adrenergic $Ca_V1.2$ stimulation revealed by proximity proteomics. *Nature*. 577:695–700. https://doi.org/10.1038/s41586-020-1947-z

Lomize, M.A., I.D. Pogozheva, H. Joo, H.I. Mosberg, and A.L. Lomize. 2012. OPM database and PPM web server: Resources for positioning of proteins in membranes. *Nucleic Acids Res.* 40:D370–D376. https://doi.org/10.1093/nar/gkr703

Lomize, A.L., S.C. Todd, and I.D. Pogozheva. 2022. Spatial arrangement of proteins in planar and curved membranes by PPM 3.0. *Protein Sci.* 31: 209–220. https://doi.org/10.1002/pro.4219

Puhl, H.L. III, V.B. Lu, Y.-J. Won, Y. Sasson, J.A. Hirsch, F. Ono, and S.R. Ikeda. 2014. Ancient origins of RGK protein function: Modulation of voltage-gated calcium channels preceded the protostome and deuterostome split. *PLoS One*. 9:e100694. https://doi.org/10.1371/journal.pone.0100694

Madhvani, R.V., Y. Xie, A. Pantazis, A. Garfinkel, Z. Qu, J.N. Weiss, and R. Olcese. 2011. Shaping a new Ca^{2+} conductance to suppress early afterdepolarizations in cardiac myocytes. *J. Physiol.* 589:6081–6092. https://doi.org/10.1113/jphysiol.2011.219600

Madhvani, R.V., M. Angelini, Y. Xie, A. Pantazis, S. Suriany, N.P. Borgstrom, A. Garfinkel, Z. Qu, J.N. Weiss, and R. Olcese. 2015. Targeting the late component of the cardiac L-type Ca2+ current to suppress early afterdepolarizations. *J. Gen. Physiol.* 145:395–404. https://doi.org/10.1085/jgp.201411288

Magyar, J., C.E. Kiper, G. Sievert, W. Cai, G.-X. Shi, S.M. Crump, L. Li, S. Niederer, N. Smith, D.A. Andres, and J. Satin. 2012. Rem-GTPase regulates cardiac myocyte L-type calcium current. *Channels*. 6:166–173. https://doi.org/10.4161/chan.20192

Maleckar, M.M., A.G. Edwards, W.E. Louch, and G.T. Lines. 2017. Studying dyadic structure-function relationships: A review of current modeling approaches and new insights into Ca^{2+} (mis)handling. *Clin. Med. Insights Cardiol.* 11:1179546817698602. https://doi.org/10.1177/1179546817698602

Manning, J.R., G. Yin, C.N. Kaminski, J. Magyar, H.Z. Feng, J. Penn, G. Sievert, K. Thompson, J.P. Jin, D.A. Andres, and J. Satin. 2013. Rad GTPase deletion increases L-type calcium channel current leading to increased cardiac contraction. *J. Am. Heart Assoc.* 2:e000459. https://doi.org/10.1161/JAHA.113.000459

Mirdita, M., K. Schütze, Y. Moriwaki, L. Heo, S. Ovchinnikov, and M. Steinegger. 2022. ColabFold: Making protein folding accessible to all. *Nat. Methods*. 19:679–682. https://doi.org/10.1038/s41592-022-01488-1

Murata, M., E. Cingolani, A.D. McDonald, J.K. Donahue, and E. Marbán. 2004. Creation of a genetic calcium channel blocker by targeted gem gene transfer in the heart. *Circ. Res.* 95:398–405. https://doi.org/10.1161/01.RES.0000138449.85324.c5

Pang, C., S.M. Crump, L. Jin, R.N. Correll, B.S. Finlin, J. Satin, and D.A. Andres. 2010. Rem GTPase interacts with the proximal CaV1.2 C-terminus and modulates calcium-dependent channel inactivation. *Channels (Austin)*. 4:192–202. https://doi.org/10.4161/chan.4.3.11867

Papa, A., S.I. Zakharov, A.N. Katchman, J.S. Kushner, B.-X. Chen, L. Yang, G. Liu, A.S. Jimenez, R.J. Eisert, G.A. Bradshaw, et al. 2022. Rad regulation of $Ca_V1.2$ channels controls cardiac fight-or-flight response. *Nat. Cardiovasc. Res.* 1:1022–1038. https://doi.org/10.1038/s44161-022-00157-y

Reynet, C., and C.R. Kahn. 1993. Rad: A member of the Ras family overexpressed in muscle of type II diabetic humans. *Science*. 262:1441–1444. https://doi.org/10.1126/science.8248782

Sasson, Y., S. Subramaniam, T. Buki, L. Almagor, O. Chomsky-Hecht, M. Katz, H. Puhl, S.R. Ikeda, N. Dascal, and J.A. Hirsch. 2022. Mapping Molecular Determinants of CaV2.2 Inhibition by RGK Proteins and Homologs in Xenopus Oocytes. *bioRxiv*. https://doi.org/10.1101/2022.06.21.496996 (Preprint posted June 24, 2022).

Satin, J. 2017. Regulation of cardiac calcium channels. In Cardiac Electrophysiology: From Cell to Bedside. D.P. Zipes, J. Jalife and W. Stevenson, editors. Elsevier, The Netherlands. 1424.

Schneider, CA., W.S. Rasband, and K.W. Eliceiri. 2012. NIH Image to ImageJ: 25 years of image analysis. *Nat Methods*. 9:671–675. https://doi.org/10.1038/nmeth.2089

Soeller, C., and M.B. Cannell. 1999. Examination of the transverse tubular system in living cardiac rat myocytes by 2-photon microscopy and

digital image-processing techniques. *Circ. Res.* 84:266–275. https://doi.org/10.1161/01.RES.84.3.266

Wang, J., P. Youkharibache, D. Zhang, C.J. Lanczycki, R.C. Geer, T. Madej, L. Phan, M. Ward, S. Lu, G.H. Marchler, et al. 2020. iCn3D, a web-based 3D viewer for sharing 1D/2D/3D representations of biomolecular structures. *Bioinformatics*. 36:131–135. https://doi.org/10.1093/bioinformatics/btz502

Wang, J., P. Youkharibache, A. Marchler-Bauer, C. Lanczycki, D. Zhang, S. Lu, T. Madej, G.H. Marchler, T. Cheng, L.C. Chong, et al. 2022. iCn3D: From web-based 3D viewer to structural analysis tool in batch mode. *Front. Mol. Biosci.* 9:831740. https://doi.org/10.3389/fmolb.2022.831740

Ward, Y., B. Spinelli, M.J. Quon, H. Chen, S.R. Ikeda, and K. Kelly. 2004. Phosphorylation of critical serine residues in Gem separates cytoskeletal reorganization from down-regulation of calcium channel activity. *Mol. Cell. Biol.* 24:651–661. https://doi.org/10.1128/MCB.24.2.651-661.2004

Weiss, S., S. Oz, A. Benmocha, and N. Dascal. 2013. Regulation of cardiac L-type Ca^{2+} channel CaV1.2 via the β-adrenergic-cAMP-protein kinase A pathway: Old dogmas, advances, and new uncertainties. *Circ. Res.* 113:617–631. https://doi.org/10.1161/CIRCRESAHA.113.301781

Westhoff, M., and R.E. Dixon. 2021. Mechanisms and regulation of cardiac $Ca_V1.2$ trafficking. *Int. J. Mol. Sci.* 22:22. https://doi.org/10.3390/ijms22115927

Yang, T., X. Xu, T. Kernan, V. Wu, and H.M. Colecraft. 2010. Rem, a member of the RGK GTPases, inhibits recombinant CaV1.2 channels using multiple mechanisms that require distinct conformations of the GTPase. *J. Physiol.* 588:1665–1681. https://doi.org/10.1113/jphysiol.2010.187203

Yang, T., A. Puckerin, and H.M. Colecraft. 2012. Distinct RGK GTPases differentially use α1- and auxiliary β-binding-dependent mechanisms to inhibit CaV1.2/CaV2.2 channels. *PLoS One*. 7:e37079. https://doi.org/10.1371/journal.pone.0037079

Zacchigna, S., A. Paldino, I. Falcão-Pires, E.P. Daskalopoulos, M. Dal Ferro, S. Vodret, P. Lesizza, A. Cannatà, D. Miranda-Silva, A.P. Lourenço, et al. 2021. Towards standardization of echocardiography for the evaluation of left ventricular function in adult rodents: A position paper of the ESC working group on myocardial function. *Cardiovasc. Res.* 117:43–59. https://doi.org/10.1093/cvr/cvaa110

Supplemental material

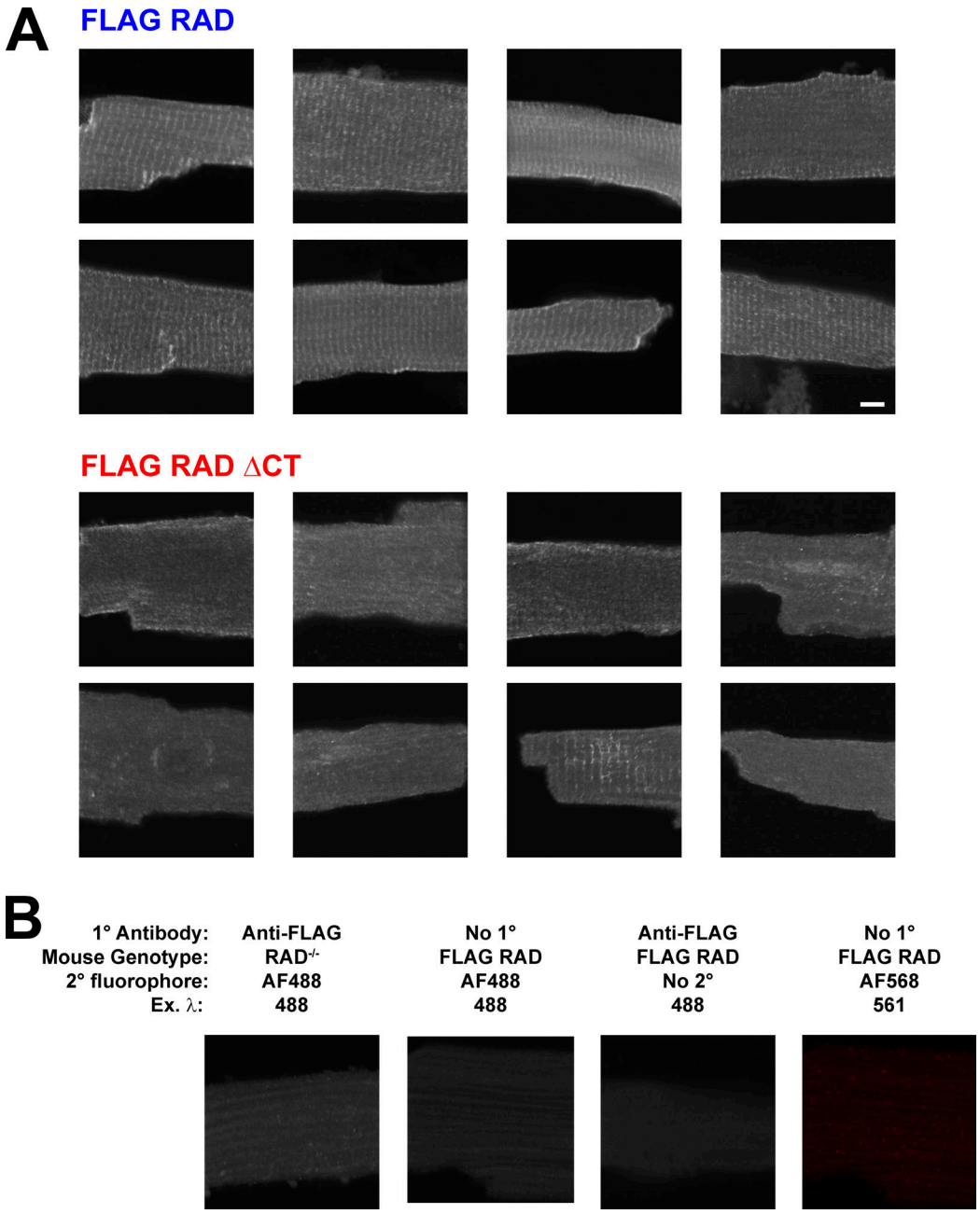

Figure S1. **Confocal micrographs of fixed adult murine ventricular cardiomyocytes immunostained with anti-Flag antibody to detect Flag-Rad localization. (A)** Cells were β-adrenergic receptor agonist treated isolated from transgenic mice with full-length Flag-Rad (*N* = 3 mice, *n* = 8 cells displayed) or Flag-RadΔCT (*N* = 3 mice, *n* = 8 cells displayed), representative of a total of 6 and 6 mice, 41 and 41 cells, and 93 and 92 images. Note that the bottom right Flag-RadΔCT image showing t-tubular expression is from the same cell in Fig. 2, representative of the observation that 7% of Flag-RadΔCT cells show t-tubular like expression in at least one region, but not regularly throughout the entire cell (0%). Scale bar, 5 µm; magnification is the same for all images. **(B)** Confocal microscopy controls were imaged and stained with the same protocols and with the same visualization background and contrast adjustments. For controls of the anti-Flag Rad antibody, a cardiomyocyte from a Rad knockout mouse ($Rad^{-/-}$) was imaged along with a Flag-Rad cardiomyocyte incubated with no primary antibody imaged with the same settings used for anti-Flag-Rad acquisition. Additionally, a Flag-Rad cardiomyocyte was incubated with no secondary antibody (no fluorophore) and imaged. Lastly, as a control for the commercial $Ca_V1.2$ antibody (image presented in Fig. 2 C), a no primary anti-$Ca_V1.2$ antibody incubated Flag-Rad cardiomyocyte was imaged the same settings used for $Ca_V1.2$ imaging.

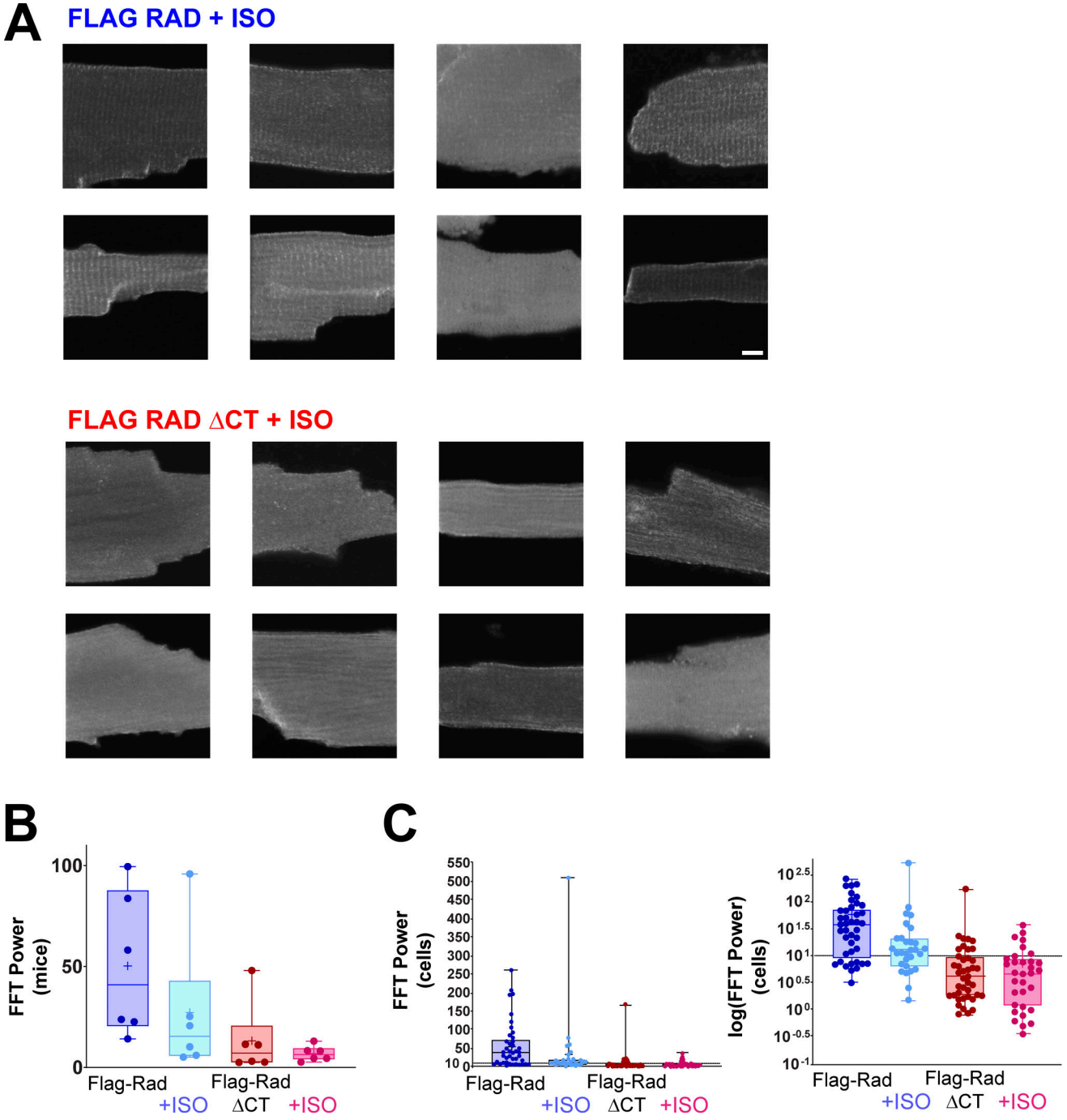

Figure S2. **Confocal micrographs of fixed adult murine ventricular cardiomyocytes treated with 1 µM ISO for 3 min and immunostained with anti-Flag antibody to detect Flag-Rad localization. (A)** Cells were isolated from the hearts of transgenic mice expressing full-length Flag-Rad (*N* = 6 mice, *n* = 8 cells displayed) or Flag-RadΔCT (*N* = 6 mice, *n* = 8 cells displayed), representative of 6 and 6 mice, 29 and 32 cells, and 64 and 62 images. Scale bar, 5 µm; magnification is the same for all images. **(B)** Fundamental peak power of anti-Flag immunostaining that represents a signal with periodicity consistent with t-tubular expression of both genotypes and ±ISO. In A and Fig. 5 B, the data is plotted on a linear y-axis here instead of log10. **(C)** The individual cell data points are shown that were averaged for the mouse data, both in linear and $\log_{10}$ scale. A line in both graphs at FFT Power 10 is denoted, corresponding to the proportions of cells over 10 shown in Fig. 2 C and Fig. 5 E. Note that for cells, the 75th percentile of both Flag-RadΔCT groups are below this threshold of 10 FFT Power.

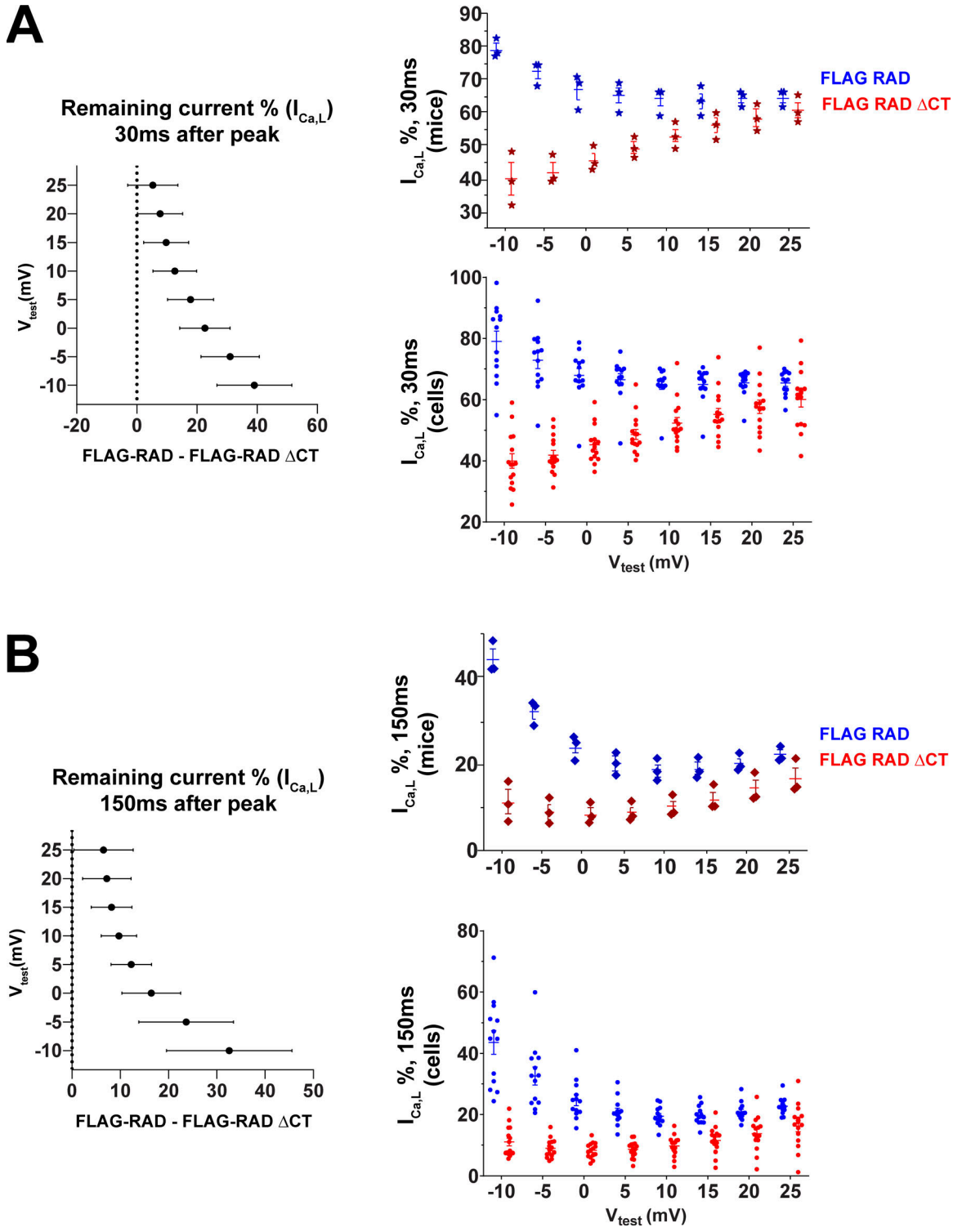

Figure S3. **Flag-RadΔCT cardiomyocytes display faster $I_{Ca,L}$ decay kinetics. (A and B)** Confidence intervals of differences between genotypes at a given V_{test} was calculated from cells for (A) percent remaining current 30 milliseconds after peak current and (B) current 150 ms after peak current. Individual mice and cell data points are plotted that represent the averages shown in Fig. 4, B and C.

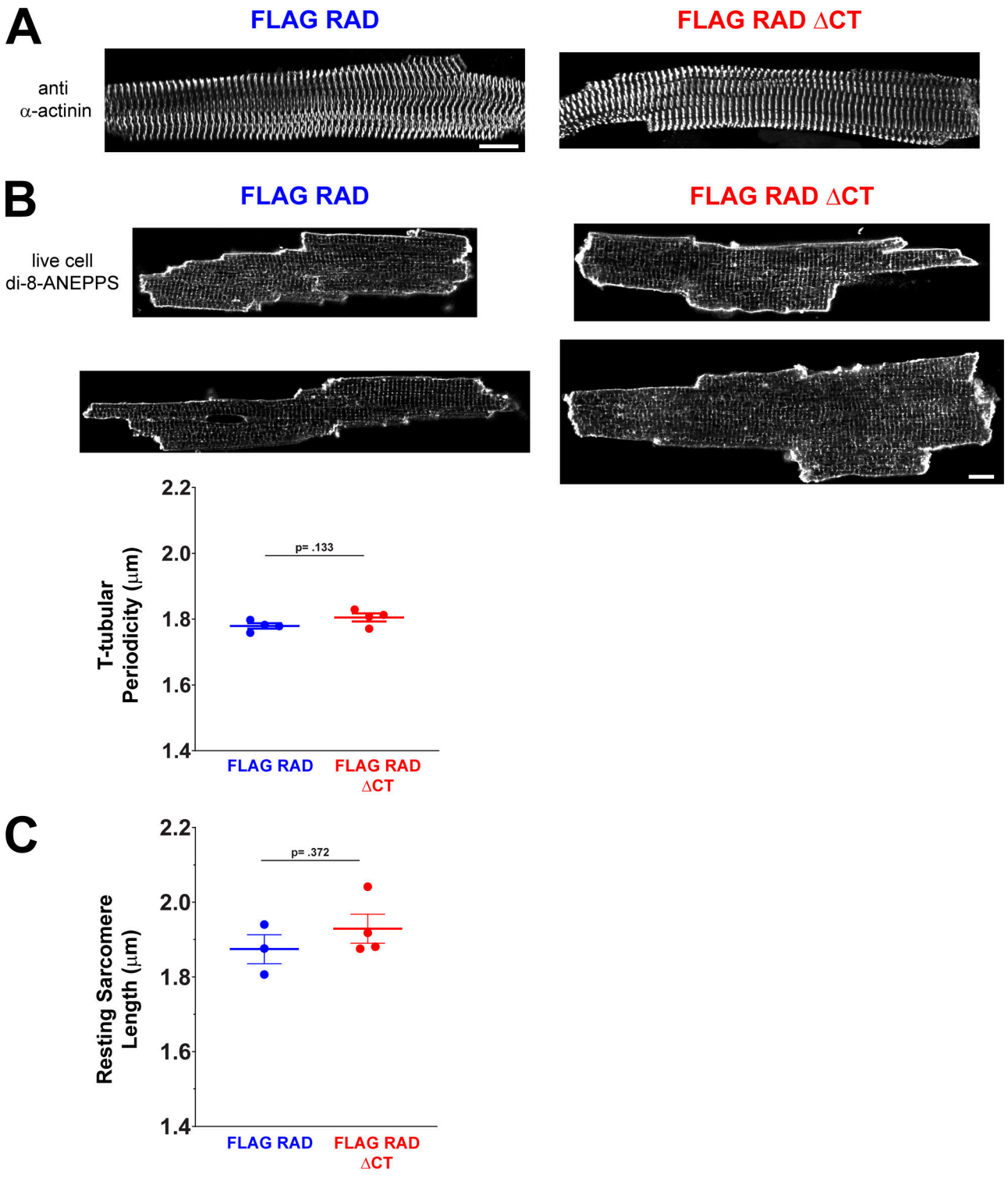

Figure S4. **T-tubule integrity in Flag-Rad and Flag-RadΔCT cardiomyocytes. (A)** Representative α-actinin staining of Flag-Rad and Flag-RadΔCT cardiomyocytes. Scale bar, 10 µm; magnification is the same for both panels. **(B)** Live cardiomyocyte di-8-ANEPPS staining of representative cardiomyocytes. FFT analysis of t-tubule periodicity did not vary significantly between genotypes (mean spacing 1.78 [SEM = 0.008] and 1.81 [SEM = 0.012] µm, for Flag-Rad and Flag-RadΔCT, respectively) (linear mixed model, nesting cells into mice, genotype F = 3.058, P = 0.133, *N* = 8 mice, *n* = 127 cells). Scale bar, 10 µm; magnification is the same for all panels. **(C)** FFT analysis of resting sarcomere length from brightfield microscopy of live cells did not vary significantly between genotype (mean spacing 1.87 [SEM = 0.0385] and 1.93 [SEM = 0.0388] µm, for Flag-Rad and Flag-RadΔCT) (linear mixed model, nesting cells into mice, genotype F = 0.958, P = 0.372, *N* = 7 mice, *n* = 122 cells).

Video 1. **SR SIM of maximal intensity projection (multiple z-slices) of Flag-Rad stained with Flag antibody.** Scale x = 32.9 µm; y = 32.9 µm;, z = 4.1 µm.

Video 2. **SR SIM of maximal intensity projection (multiple z-slices) of Flag-RadΔCT stained with Flag antibody.** Scale x = 32.9 µm; y = 32.9 µm;, z = 4.9 µm.

Video 3. **Alphafold full-length Rad (Uniprot accession no.** O88667**) PPM 3.0 computational model of interaction with plasma membrane**.